Proposal for a

STUDY OF QED AT CRITICAL FIELD STRENGTH

IN INTENSE LASER–HIGH ENERGY ELECTRON COLLISIONS

AT THE STANFORD LINEAR ACCELERATOR

C. Bula, K.T. McDonald, E.J. Prebys and D. Strozzi
Joseph Henry Laboratories, Princeton University, Princeton, NJ 08544

C. Bamber[(1)], S. Boege[(1)], T. Koffas[(1)], T. Kotseroglou[(1)], A.C. Melissinos[(1)], D. Meyerhofer[(2)], D. Reiss[(1)] and W. Ragg[(1)]
Department of Physics[(1)], Department of Mechanical Engineering[(2)], University of Rochester, Rochester, NY 14627

D.L. Burke, P. Chen, R.C. Field, G. Horton-Smith, A.C. Odian, J.E. Spencer, D. Walz and M.S. Woods
Stanford Linear Accelerator Center, Stanford University, Stanford, CA 94309

S. Berridge, W.M. Bugg, K. Shmakov and A.W. Weidemann
Department of Physics and Astronomy
University of Tennessee, Knoxville, TN 37996

Proposed October 20, 1991

Conditional approval as Experiment 144 on December 20, 1991

Full approval on September 30, 1992

Executive Summary

We propose a program of study of the interaction of electrons and photons in fields approaching the critical QED field strength of an electron rest energy per Compton wavelength. This can be achieved in collisions between the picosecond pulses of a teraWatt laser and a 50-GeV electron beam. The phenomena accessible to study include nonlinear Compton scattering, trident production, and Breit-Wheeler pair production. The electric field at the laser focus is of similar strength to that of an electron bunch in future linear colliders, permitting a close analog of beamstrahlung to be studied. Measurement of the invariant-mass spectrum of electron-positron pairs could clarify whether the positron peaks seen at Darmstadt in heavy-ion collisions are a strong-field QED effect. Electron-laser collisions at critical field strength may prove to be a high-brightness source of positrons for future colliders.

Contents

1 Introduction **1**

2 Experimental Setup **3**
2.1 Overview . . . 3
2.2 Beam Parameters and Event Rates . . . 6
2.3 The Laser Interaction Points . . . 10
2.4 The Detector . . . 11
2.5 Backgrounds . . . 13

3 Nonlinear Compton Scattering **14**

4 Beamstrahlung **17**

5 The Multiphoton Breit-Wheeler Process **17**

6 The e^+e^- Mass Spectrum in High Fields **21**

7 The Laser System **26**

8 Appendix A: The e-ω and γ-ω Interaction Regions **30**

9 Appendix B: Synchrotron Radiation **31**

10 References **34**

List of Figures

1 The FFTB beamline downstream of the final focus. . . . 4
2 Proposed layout of the interaction region. . . . 5
3 Backscattered photon spectrum for $\lambda = 350$ nm and $E_e = 50$ GeV. . . . 8
4 Schematic of the laser-interaction points. . . . 11
5 Schematic of the pair-spectrometer layout. . . . 12
6 The pair-spectrometer acceptance. . . . 12
7 Cross section for Compton scattering of 50-GeV electrons. . . . 16
8 Cross section *vs.* E_γ for the Breit-Wheeler process. . . . 19
9 Cross section *vs.* η for the Breit-Wheeler process. . . . 20
10 Cross section *vs.* E_e for the Breit-Wheeler process. . . . 20
11 Darmstadt positron peaks. . . . 21
12 Preliminary results from high-energy-γ channeling in crystals. . . . 22
13 Pair-production rate *vs.* electron energy. . . . 23
14 Pair-production rates *vs.* number of laser photons. . . . 24
15 Pair-production rate *vs.* pair mass. . . . 25
16 Chirped-pulse amplification and compression. . . . 27
17 Achieved laser performance. . . . 28

1 Introduction

We propose to study the scattering of 50-GeV electrons from a focused short pulse of UV light ($\lambda = 350$ nm) with peak energy flux $I \sim 4 \times 10^{18}$ W/cm^2. At this energy density, the Lorentz-invariant ratio of the electric field $E^\star = \gamma E$ seen by the electron to the QED critical field $E_{\rm crit} = m^2c^3/e\hbar$ [1, 2],

$$\Upsilon \equiv \frac{E^\star}{E_{\rm crit}} = 2\gamma\,\frac{eE\hbar}{m^2c^3}, \tag{1}$$

approaches unity. In this region, perturbative QED is of limited validity and one expects copious production of e^+e^- pairs and the dominance of multiphoton effects [3].

More generally, multiphoton effects become important in a wave field of frequency ω when the parameter

$$\eta \equiv \frac{eE}{\omega mc} \tag{2}$$

approaches or exceeds unity. This (Lorentz-invariant) parameter is proportional to the magnitude of the classical vector potential of the wave field, and characterizes the transverse velocity induced on an electron by the wave. When this velocity approaches c higher multipole radiation predominates, corresponding to multiphoton absorption in a quantum description. Multiphoton-absorption processes have been observed with atomic electrons but not with high-energy free electrons.

If the incident wave is circularly polarized, then the electron's motion is a helix of radius r, and we can introduce a transverse velocity $\beta_\perp$ and a transverse relativistic factor $\gamma_\perp$ through an analysis in the average rest frame of the electron:

$$eE^\star = \gamma_\perp m\omega^{\star 2} r = \gamma_\perp \beta_\perp m\omega^\star c, \tag{3}$$

where

$$\beta_\perp = \frac{v_\perp}{c} = \frac{\omega^\star r}{c} \qquad\qquad \gamma_\perp = \left(1-\beta_\perp^2\right)^{-1/2}. \tag{4}$$

Therefore the parameter η of Eq. (2) can be written as

$$\eta = \gamma_\perp\beta_\perp \qquad\qquad \text{and} \qquad\qquad \gamma_\perp = \left(1+\eta^2\right)^{1/2}. \tag{5}$$

Due to its transverse motion in the field the electron acquires an "effective mass"

$$\overline{m}^2 = m^2\gamma_\perp^2 = m^2\left(1+\eta^2\right). \tag{6}$$

In a quantum description one does not refer to the classical path of the transverse motion of the electron in the wave field, but rather the Volkov solutions to the Dirac equation [4]. The kinematic character of these solutions can be summarized by writing the four-vector of the electron as

$$\overline{p}_\mu = p_\mu + \kappa\omega_\mu, \tag{7}$$

where p_μ is the four-vector of the electron in the absence of the wave, ω_μ is the four-vector of a wave photon, and $\kappa = \eta^2 m^2/2(p\cdot\omega)$. The latter relation follows from setting $\overline{p}^2 = \overline{m}^2$. Loosely speaking, an electron in a wave field has absorbed κ wave photons. If an electron or positron is created in the field, its invariant mass is immediately $\overline{m}$, which relaxes to m only when the particle leaves the wave field.

In the proposed studies of strong-field QED we will simultaneously explore the two nonlinear effects of multiphoton absorption, and of vacuum polarization. While the case of $\eta \approx 1$ can be realized in low-amplitude, long-wavelength fields, the parameter Υ can approach 1 with present-day lasers only when probed with electrons of 50-GeV energy. In principle, $\Upsilon \sim 1$ can also be reached in heavy-ion collisions [5] when the Z of the combined nuclei satisfies $\alpha Z > 1$, and in channeling of very high-energy electrons through thin crystals [6]. Beamstrahlung at future linear colliders is another situation in which Υ can easily exceed unity which strongly influences their design. It can be shown explicitly [3] that when η approaches or exceeds unity, the underlying physics of multiphoton processes is similar to that that occurs in a static field at the same value of Υ.

This proposal involves four related measurements which can be carried out in the C-line as it is being set up to deliver a low-emittance 50-GeV beam (the Final Focus Test Beam, FFTB). All four experiments use the same apparatus with only minor modifications and are a natural progression in a systematic test of QED at critical field strength. The experiments are of increasing complexity and their goals are correspondingly more ambitious, as follows:

(a) Nonlinear (multiphoton) Compton scattering. For this experiment the laser wavelength is not important and for simplicity we will use infrared ($\lambda = 1,054$ nm). The principal demand on the electron beam is that it be parallel (to within few microradians), whereas the intensity need only exceed 10^7/pulse. Apart from its intrinsic interest, this experiment is also a pilot for the generation of an intense high-energy gamma beam needed for measurements (c) and (d). A study of nonlinear Compton scattering using 50-MeV electrons is presently underway at BNL [7].

(b) Measurement of the energy spectrum of the positrons emerging from the e-ω collision and of the energy and angular distribution of wide angle (up to 100 microradians) high energy γ's. These can be produced in multiphoton interactions typical of the beamstrahlung process [7]. The values of Υ achieved in the experiment are of the same order as in the next generation of linear colliders. For this measurement we will use both IR and UV laser pulses.

(c) Measurement of pair production in γ-γ scattering with both photons real:

$$n\omega_0 + \omega \rightarrow e^+e^-. \tag{8}$$

This is the multiphoton version of the Breit-Wheeler process [9] where ω_0 is an incident laser photon and ω is a high-energy photon derived from backscattering the laser photons ω_0 off the electron beam [10, 11]. We will use a UV ($\lambda = 350$ nm) pulse, which yields high-energy photons with $\omega_{\max} = 36.5$ GeV. The expected flux in the upper 10%

of the energy band is $\gtrsim 10^5$/pulse. Part of the UV pulse is brought in collision with the electrons to produce the high-energy photons, whereas the remainder of the UV pulse is tightly focused and brought in collision with the high-energy photons. For a UV laser at SLAC, we need to absorb at least three laser photons to make an e^+e^- pair.

(d) Measurement of the mass spectrum of the e^+e^- pairs produced in reaction (8), with a resolution of 10 keV in the low-mass region, $M \sim$ 1.0-2.0 MeV/c^2. This is the region where the Darmstadt experiments have observed peaks in the e^+e^- effective mass [5]. A possible explanation for this structure is that it is associated with the high fields present during the heavy-ion collision; similar field strengths are present in our experiment. Two experiments have demonstrated that there are no resonances in e^+e^- scattering in a field-free region [12, 13]. Some authors have speculated that at high fields QED undergoes a phase transition to a confining state, which would have bound e^+e^- states [14]. Our experiment offers the best opportunity at the present time to test these conjectures in the laboratory free from the complications of the strong interaction.

The production of positrons by direct pair production in multiphoton-electron interactions, or by multiphoton-electron scattering followed by reaction (8) [15] could have a major impact on the performance of future linear e^+e^- colliders. The luminosity of such colliders is limited by the brightness of the electron and positron sources used, and these, in present designs, are limited by the brightnesses that can be generated in damping rings. Electron beams of greater brightness can be generated in rf photocathode guns, but if positrons are made from the electrons by pair production in targets then their emittance is relatively large, due in part to multiple Coulomb scattering in the target. A damping ring must then be used, at least for the positrons, and this limits the luminosity. If multiphoton-electron interactions are used to generate the positrons then their emittance will be little greater than that of the initial electrons as there is no ill effect of multiple Coulomb scattering here. For very intense laser beams and electron energies of $\sim$ 100 GeV the laser pulse can be effectively one radiation length, so the brightness of the electron beam could be largely preserved, no damping rings would be required, and the potential luminosity of the collider could be raised.

Finally it has been recognized for a long time that linear e^+e^- colliders could also be operated as γ-e or γ-γ colliders [16, 17, 3]. The high-energy γ-beam is best provided by backscattering of an intense short laser pulse. The present experiments will demonstrate the technique whereby nearly 100% of an electron beam can be converted to high-energy photons. It would then be of interest to evaluate the applicability of this technique to the SLC under its present operating conditions.

2 Experimental Setup

2.1 Overview

The experimental set up consists of the incident electron beam, the laser system and of a suitable interaction point where the laser pulse can be brought into collision with the electron

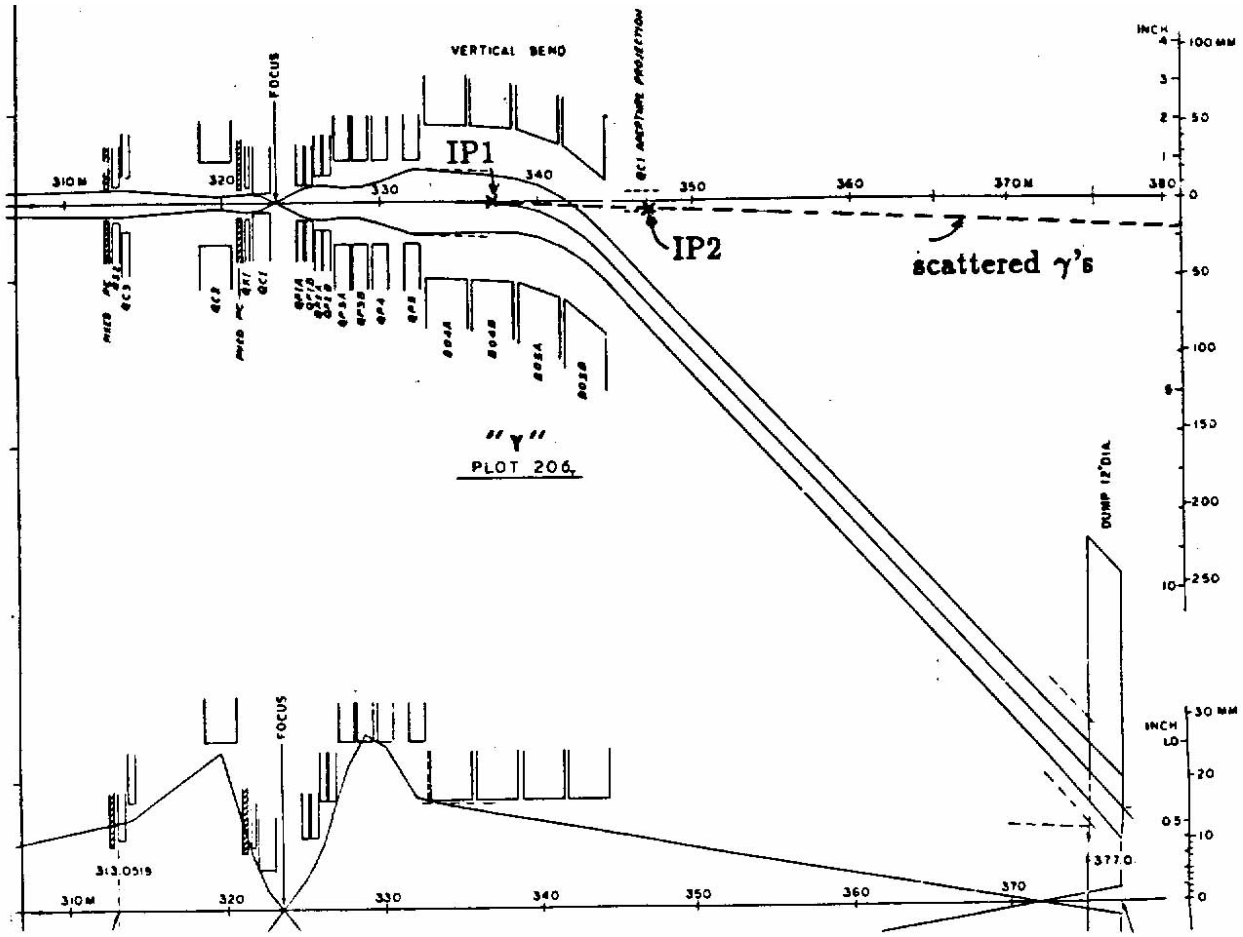

Figure 1: The present design of the FFTB beamline downstream of the final focus. The locations of the proposed laser-electron (IP1) and γ-laser (IP2) interaction regions are indicated.

bunch. A second interaction point is necessary further downstream to bring the laser pulse into collision with the high-energy backscattered γ's. The principal detector is a magnetic pair spectrometer located approximately 100 m from the interaction points. The inclusive spectrum of the e^+ produced in the e-ω collisions will be measured with a silicon calorimeter near the first interaction point.

The FFTB downstream its final focus is well suited for the proposed experiments. The section of beam optics that transports the FFTB to its dump is shown in Fig. 1. The proposed arrangement, shown in Fig. 2, contains three soft bends one of 400-μrad and two of 50μrad; these are followed by an 18 mrad hard bend which directs the beam to the dump. The focussing elements have sufficient strength to make a parallel beam or to bring the beam to a focus at the first interaction point (IP1). The IP1 is located between the two 50-μrad bends so that the scattered γ's and e^+e^- pairs do not propagate along the beamline with its higher energy synchrotron radiation.

The scattered particles are transported in a (2-4) inch diameter vacuum pipe from the

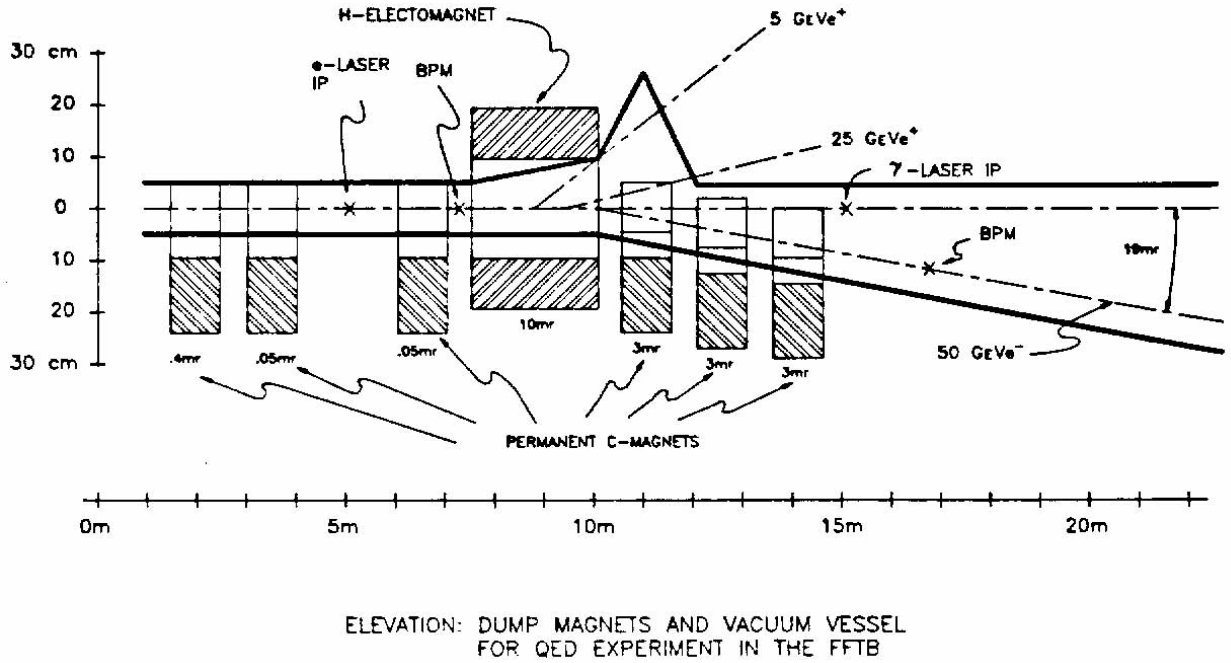

Figure 2: Proposed layout of the interaction region.

interaction point to the detector, 100 m downstream. This pipe clears the beam dump and its muon shielding and there exists sufficient space for its installation. The vertical-deflection magnets for the beam serve the additional function of sweeping all secondary charged particles out of the forward direction. If the beam angular divergence is kept below 10 μr, the spot size of the high-energy neutrals at the detector is of order ± 2 mm. The distance from the IP to the spectrometer has been chosen so as to provide adequate angular resolution for the measurement of the pair effective mass, but also such that the background rate can be reduced to less than 1 count/pulse in any one detector plane.

For the photon-photon (γ-ω) scattering experiments, a second interaction point (IP2) is necessary. This is located 10 m downstream from IP1. The two interaction regions are of exactly the same design and must be isochronous since a fraction of the same laser pulse is directed at each of them.

The inclusive spectrum of the positrons produced in the electron-laser collision is measured inside the beam enclosure. Positrons are dispersed in the vertical plane by the beam-transport dipoles which are open on the upper half (C magnets). The positrons are detected by a silicon calorimeter which also provides position information. The acceptance of the calorimeter covers positron momenta $5 < P_+ < 25$ GeV/c and the correlation between the magnetic and calorimetric measurement will be used to reject background. The expected real event rate is of order of 1/pulse or less.

2.2 Beam Parameters and Event Rates

We assume the following parameters for the uncoupled electron beam:

$$\begin{aligned} \text{Invariant emittance } \gamma\epsilon_x &= 3\times10^{-5} \text{ m-rad } (\epsilon_y = \epsilon_x/10) \\ \text{Electron energy} &= 50 \text{ GeV} \\ \text{Electrons per pulse} &= 10^9\text{-}10^{10} \\ \text{Bunch length} &= 500\ \mu\text{m} \end{aligned}$$

Even though the beam repetition rate is 10 Hz, the laser system can deliver only 1 Hz [18] and all event rates are calculated on that basis. In general the experiment can run parasitically off the FFTB since the desired beam optics can be established without affecting the final focus. In Table 1 below we list possible beam optics for a parallel, and a point focus beam at IP1, as well as for the nominal low-β beam.

Note that in general the laser beam is focused to an area smaller than the electron beam, and thus the rate of backscattered high energy γ's can be estimated from

$$N_\gamma = \frac{N_e}{A_e}\,\sigma_{_C} N_L, \tag{9}$$

where

$$\begin{aligned} N_e &= \text{Number of electrons in bunch} \\ A_e &= \text{Area of electron bunch} \\ N_L &= \text{Number of photons in laser pulse} \\ \sigma_{_C} &= \text{Compton cross section} \end{aligned}$$

Table 1: Parameters of three beamline options for interaction point IP1 in the FFTB.

Parameter	FFTB Beam Tune		
	Nominal Low-β	Parallel	Point Focus
$\sigma_{x/y}$ (μm) at the FF	0.95/0.055	0.95/0.055	30/20
$\sigma_{x,\max}$ (μm) after FF (quad QP3)	2730	2700	121
$\sigma_{y,\max}$ (μm) after FF (quad QP5)	2883	2479	65
$\sigma_{x/y}$ (μm) at IP1	2314/1601	2479/1815	75/57
$\sigma_{x'/y'}$ (μrad) at IP1	54/88	1.0/0.5	3.2/6.6

and in our energy range $\sigma_{_C} \simeq 5\times10^{-25}$ cm^2. The interaction rate depends also on the relative length of the electron and laser pulses and only weakly on the crossing angle. The longitudinal extent of the laser focal region σ_ω is determined by the smaller of the confocal parameter $z_0 = 2.28\lambda(f/D)^2$, and the pulse length. Typically, for a tight focus where

$(f/D) \sim 3$, z_0 is much smaller than the length of a 1-ps laser pulse. Synchronization of the two beams must be maintained at the 1-ps level.

For the nonlinear Compton scattering experiment the electron beam would be as for the Parallel case in Table 1. We assume $\sigma_{x'} = \sigma_{y'} = 10^{-6}$ rad and $\sigma_x = \sigma_y = 2000$ μm. The laser is focused with an $f/D = 3$ lens to a focal spot characterized by

$$\sigma_0 = 0.43\lambda(f/D) = 1.4\mu\text{m} \tag{10}$$

for $\lambda = 1054$ nm ($h\nu = 1.17$ eV). The interaction rate under these conditions and for a laser pulse energy of 0.16 Joule is 2×10^{-7}/electron. Thus for a flux of 10^9 electrons the scattered rate $N_\gamma \sim 200$. To prevent saturation of the detector we will use a thin converter to control the rate of events that are measured in every pulse; detuning of the electron beam can also be used to control the event rate. We cannot reduce the laser intensity to reduce the interaction rate without even more greatly reducing our sensitivity to nonlinear QED effects.

For the simulation of the beamstrahlung we need to approach $\Upsilon = 1$ which can be done by increasing the laser pulse energy, and also by focusing the laser beam as tightly as possible. For the latter it is be advantageous to use UV light obtained from the IR by frequency tripling. Furthermore to maximize the rate of positrons the electron beam will be focused to match the laser pulse as much as possible. Under the conditions discussed in section 4 one expects

$$n_p = 2 \times 10^{-8}/\text{electron} \tag{11}$$

where n_p is the number of pairs produced. Thus the positron rate is adequate even for 10^9 electrons/pulse. If the rate is too high for the calorimeter, it can be controlled by defocusing the electron beam.

For the γ-γ experiments the demands on the electron beam and on the laser are more stringent. It is now essential to use the UV pulse in order to achieve high energy for the backscattered γ's; furthermore one wishes to maximize their flux while also bringing them to a focus at the point of the second interaction. Thus the laser at the first interaction should **not** be tightly focused since we are not interested in nonlinear effects when producing the high-energy γ's.

Note that the transverse dimensions of the backscattered high-energy γ-beam are those of the focused laser spot at interaction point IP1, that is of the order of a 100 μm. Furthermore the high-energy part of the γ-beam follows the direction of the electron beam and therefore remains parallel to a few parts in 10^{-6}. For example, the small-angle approximation to the exact kinematic relation (18) is

$$E_\gamma \approx \frac{4\gamma^2\omega_0}{1 + 4\gamma\omega_0/m + (\gamma\theta)^2} = \frac{36.5 \text{ GeV}}{1 + (\gamma\theta/1.95)^2}, \tag{12}$$

for a 50-GeV electron beam colliding with a laser pulse of wavelength 0.351 μm. The energy spectrum of the scattered γ's is shown in Fig. 3, where the dashed line indicates the limiting energy for γ's scattered at an angle smaller than $\theta = 6 \times 10^{-6}$ rad; this region contains energies within 9% of the peak energy.

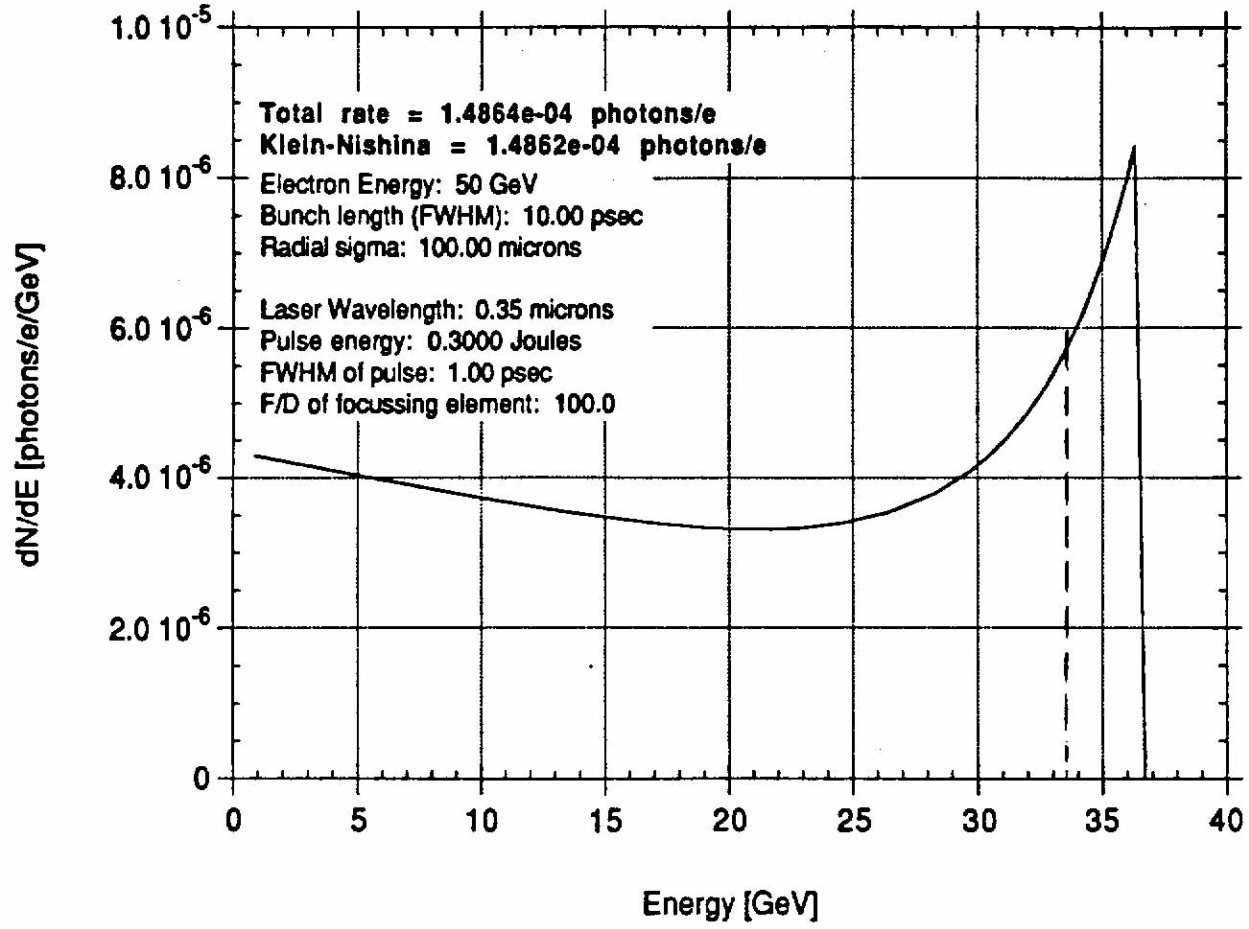

Figure 3: The spectrum of the backscattered photons when a laser pulse of $\lambda = 350$ nm is incident on 50-GeV electrons.

To scatter the high-energy γ's off the focused laser beam a second interaction point (IP2) is chosen. This is shown in Fig. 2 at a distance of $L = 10$ m from the production point of the γ's. In traveling from the production point to the γ-ω interaction region the high-energy γ's will be spread out due to the geometric divergence (or convergence) of the parent electron beam and also because of the scattering angle. If we wish to accept an energy bite ΔE at the second interaction region, we must accept a range of Compton scattering angles $\Delta\theta$, where

$$\left(\frac{\gamma\Delta\theta}{1.95}\right)^2 = \frac{\Delta E}{E}, \tag{13}$$

according to Eq. (12). This implies that the e-ω interaction should take place over a region of radius at least $L\Delta\theta$.

The luminosity (per laser pulse) at the second (γ-ω) interaction region can be calculated as in Eq. (9) since the laser beam is tightly focused here,

$$\mathcal{L} = \frac{N_\gamma}{A_\gamma}\,\frac{\Delta E}{E}\,\frac{N_L}{2} = \frac{N_\gamma (N_L/2)^2}{A_e A_\gamma}\,\frac{\Delta E}{E}\,\sigma_C. \tag{14}$$

In this, N_γ are the γ's produced at the first interaction region, and they are contained in an area A_γ at the second interaction region. $\Delta E/E$ is the energy bite and we assume a uniform distribution in energy (which underestimates the luminosity according to Fig. 3). Finally we assume that half of the laser photons are used at each of the interaction regions.

Table 2: Requirements on the electron beam and on the laser for three configurations of the proposed experiment.

Parameter	Configuration		
	Nonlinear Compton	Beamstrahlung	$\gamma + \omega \to e^+e^-$
N_e	10^9	10^9	10^{10}
σ_x, σ_y (μm)	2000	20	100
$\sigma_{x'}, \sigma_{y'}$ (rad)	10^{-6}	10^{-4}	10^{-5}
σ_z (μm)	500	500	500
λ_L (nm)	1054	351	351
Δt_L (ps)	1.2	1.2	1.2
U_L (Joule)	0.16	0.4	0.4 (at IP1) 0.4 (at IP2)
f/D	3	3	100 (at IP1) 3 (at IP2)

We estimate A_γ from

$$A_\gamma \approx \pi\sigma_{r_2}^2 = \pi(L\Delta\theta)^2.$$

For the nearly parallel beam we are considering, A_e in Eq. (9) is almost the same as A_γ, but it is insightful to write this as

$$A_e \approx \pi\sigma_{r_2}^2 \approx \pi\frac{\epsilon^2}{\sigma_\theta^2} \approx \pi\frac{\epsilon^2}{\Delta\theta^2},$$

which introduces the emittance ϵ of the electron beam in the relevant manner. See Appendix A for more detailed considerations.

Inserting these factors in Eqs. (9,14) we obtain

$$\mathcal{L} = \frac{N_e(N_L/2)^2}{\pi^2\epsilon^2L^2}\,\frac{\Delta E}{E}\sigma_{_C}. \tag{15}$$

The quantity N_e/ϵ^2 is the brightness of the electron beam.

Using then the following parameters

$$\begin{aligned} N_e &= 10^{10} \\ N_L &= 2\times10^{17} \\ \epsilon &= 3\times10^{-10}\text{ m-rad} = 3\times10^{-8}\text{ cm-rad} \\ L &= 10\text{ m} = 10^3\text{ cm} \\ \Delta E/E &= 0.09 \\ \sigma_{_C} &= 2.5\times10^{-25}\text{ cm}^2 \end{aligned}$$

we find

$$\mathcal{L} \approx 2 \times 10^{26}\ \mathrm{cm}^{-2}\mathrm{s}^{-1}.$$

The estimated cross section for $\gamma + n\omega \to e^+e^-$ at our energies is of order $\sigma \sim 10^{-27}$ cm^2 (see Sec. 5 below) so that the event rate is comfortable. Recall that we cannot use more than one event per laser pulse. The luminosity can be further increased by increasing N_e or N_L, or by decreasing ϵ or L. The number of high-energy γ's participating in the second interaction is $N_\gamma \Delta E/E \approx 3 \times 10^5$.

We summarize in Table 2 the requirements on the electron beam and on the laser, for the three configurations:

(a) Nonlinear Compton,
(b) Beamstrahlung,
(c) γ-$\omega \to e^+e^-$.

2.3 The Laser Interaction Points

The laser is brought into collision with the electron beam at IP1. A sketch of the interaction region is shown in Fig. 4. The laser beam enters and exits the high-vacuum region through 6-inch-diameter quartz windows, and has a diameter of 5 cm at that point. It is focused onto the electron beam by metallic parabolic mirrors placed at a distance of 15 cm from the intersection point. The crossing angle is $\Delta = 12^\circ$ and during operation the edge of the mirror is at 14 mm from the center of the beamline; this corresponds to 8 σ when the beam is tuned to be parallel at the IP1. To increase the clearance the mirror can be notched in the region near the beam.

The mirrors must be remotely controlled, and the exiting beam is imaged after suitable attenuation to insure the proper quality of the focus [19]. It is desirable that the mirror structures be supported on a pier and be mechanically decoupled from the vacuum pipe. Since the focal point is of order 1 μm, corresponding positional tolerances must be maintained. The mirror holders can be oriented either vertically or horizontally depending on the penetrations for bringing in the laser beam, and on the available support structures.

The second interaction point (IP2) involves the collision of the backscattered γ's with a fraction of the laser pulse. The mirror holder is of exactly the same design and is located 10 m downstream. The alignment of the two beams is more difficult in this case since the beam-position monitor can not be used to establish the location of the high-energy γ-beam. Various procedures can be followed to facilitate the alignment, including the possibility of a flying scanning wire at the beam position.

The timing of the laser pulse with respect to the electron pulse must be maintained at the 1-ps level. The most straightforward approach is to lock the laser oscillator's acousto-optic mode-locker onto the linac frequency, and then use appropriate phase shifters to maintain synchronism. This method has been successfully used at the Brookhaven ATF. It will thus be necessary to provide a good quality rf signal at the laser hut. Furthermore, the length of the optical line from the laser oscillator, through the compression stage, and into the interaction region must be stable at the level of 100 μm; therefore an active feedback will be used to control the effective length of the line.

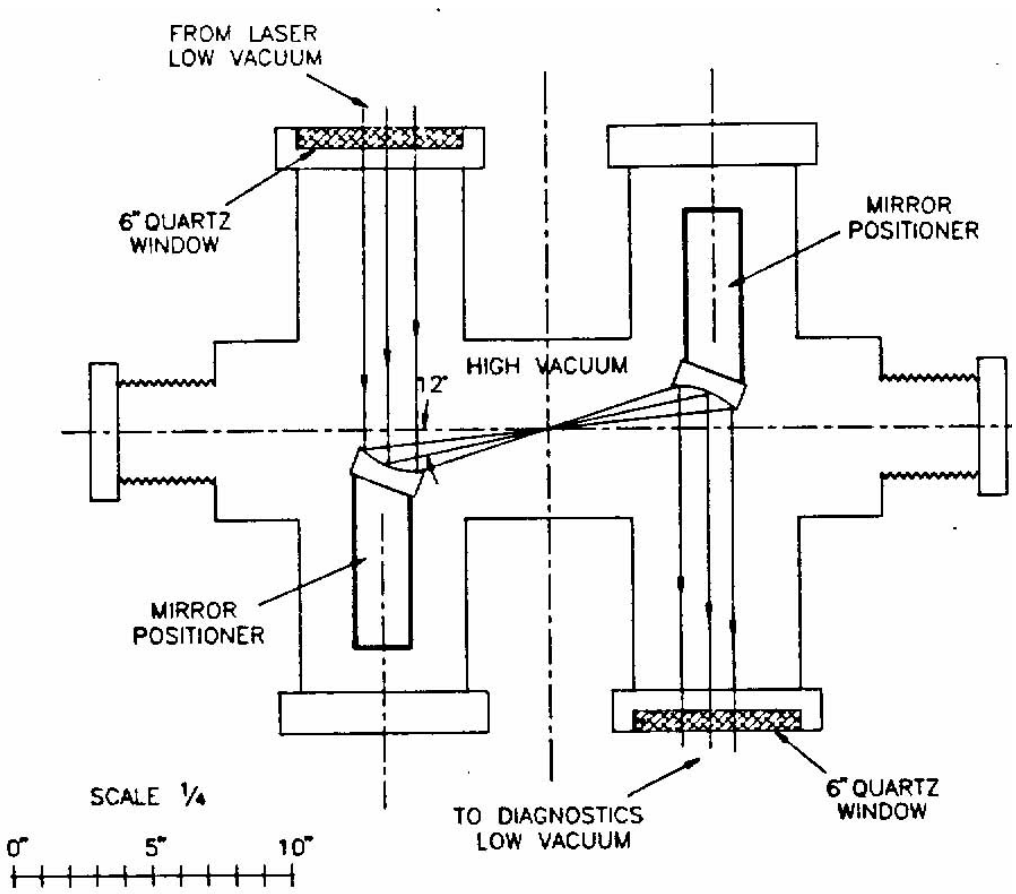

Figure 4: Schematic of the laser-interaction points.

2.4 The Detector

The detector is a pair spectrometer based on a dipole magnet with transverse kick $P_\perp = 150$ MeV/c [$\int Bd\ell = 0.5$ T-m]. The dispersion is in the horizontal plane and particle trajectories are measured using silicon CCD detectors. A schematic layout of the spectrometer is shown in Fig. 5. The acceptance will be limited to electron and positron momenta in the range $6 < P < 30$ GeV/c. This range fully covers the pair-produced e^+e^- as can be seen in Fig. 13.

To detect high-energy γ's an active silicon converter is placed upstream of the magnet as indicated in Fig. 5. The conversion efficiency will be of order $\sim 0.5\%$. The acceptance for high-energy γ's is shown in Fig. 6 and covers the region of interest, $15 < E_\gamma < 35$ GeV, with good efficiency.

The CCD's will be of the same design as used in the SLD [20]; they have an active area of 12×9 mm^2, and a 512×512 read out. Thus the pixel size is about 20 μm; the claimed resolution is of order ≈ 5 μm. To clear the secondary-photon beam the nearest edge of the CCD array will be placed at 5 mm from the beamline, and four CCD's, two on either side of the beam, will be used in each transverse plane. The CCD planes are located at 1 meter from the magnet center and are spaced by 10 cm. This allows the measurement of the trajectory

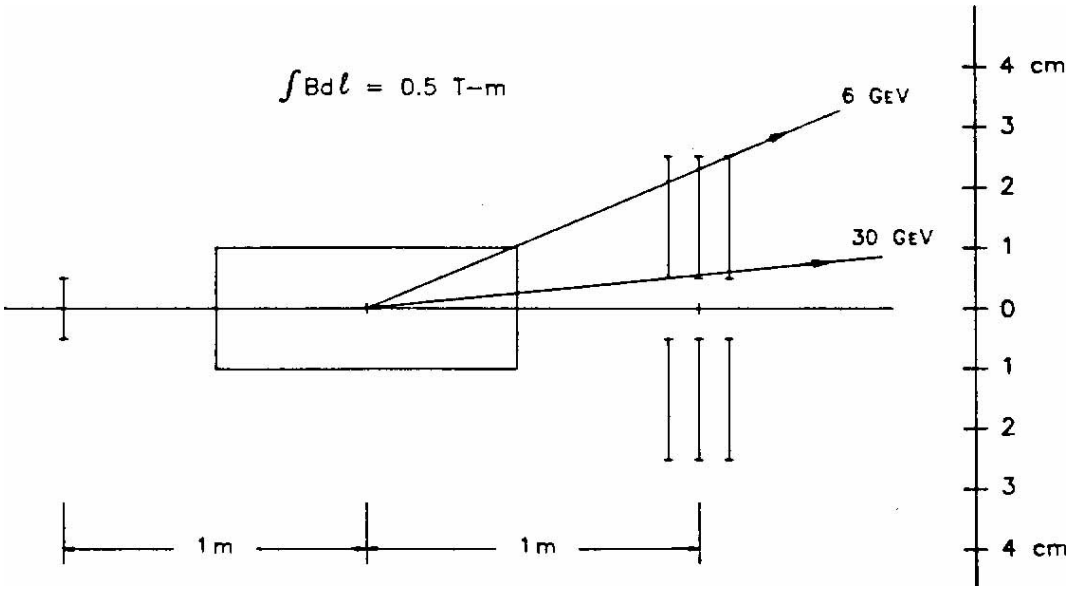

Figure 5: Schematic of the pair-spectrometer layout.

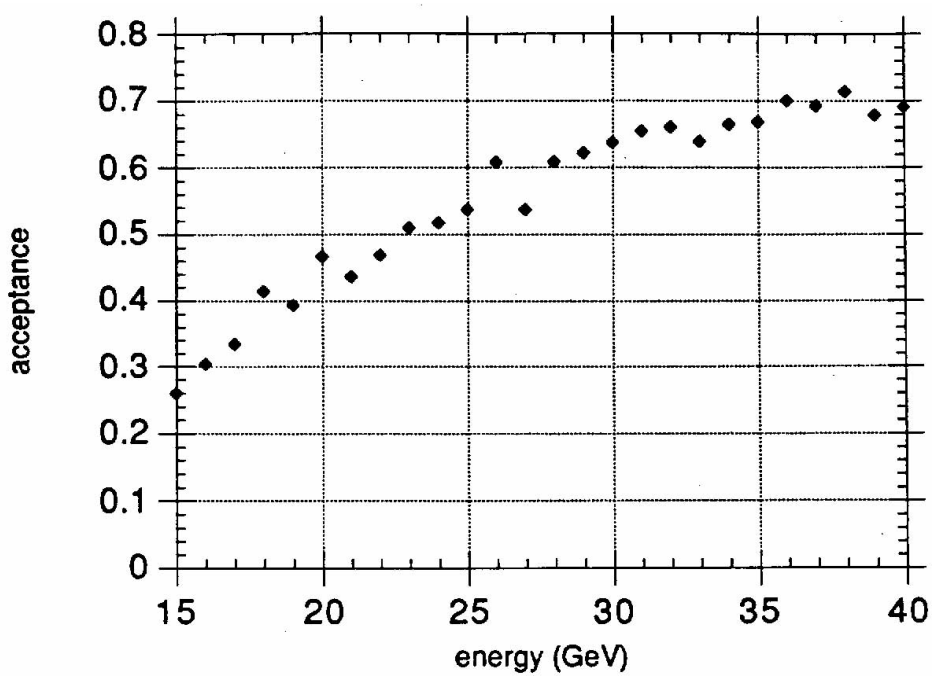

Figure 6: The pair-spectrometer acceptance for the detectors extending from $y = 4$ to $y = 30$ mm. The region of interest is $15 < E_\gamma < 35$ GeV.

angle to an accuracy $\Delta\theta = 35$ μrad, roughly equal to the multiple scattering introduced by the 200-μm-thick CCD's on the highest-energy track (30 GeV).

For the Compton experiment, the scattering angle of the γ's will be determined by the position uncertainty over the lever arm, namely to $\Delta\theta = 5$ μm/100 m $= 5 \times 10^{-8}$ rad, well below the uncertainty in the direction of the incident electron beam. The use of pixel detectors should allow the detection of multiple γ's in one event. For this, the positions of the conversion electron and positron will be matched at the center of the spectrometer magnet, 1 m upstream of the CCD tracker, with an rms error of 50 μm. But the characteristic Compton scattering angle is $1/\gamma \approx 10^{-5}$, so the backscattered photons populate a region of radius 1000 μm at the spectrometer magnet. With a requirement of 3-σ separation between photons at the spectrometer, we should be able to untangle events with up to 5-10 Compton scatters.

The high spatial resolution achieved by the CCD's will impose stringent requirements on the positional stability of the detection elements and on their alignment. The entire assembly will be in vacuum. The readout does not pose special problems since we have 1 second to record the event. Each CCD will be read serially by existing FASTBUS modules.

For the positron yield from interaction point IP1 ($5 < P_+ < 25$ GeV/c) we will use a silicon calorimeter inside the beam enclosure [21, 22]. A 2-mm segmentation in the vertical plane suffices to give $\Delta P/P = 0.03$ at $P = 25$ GeV/c, and the total area that must be covered is 15 cm in length. We will use a design similar to that of Ref. [21] consisting of 8 silicon planes interleaved with two-radiation-length-thick tungsten plates. Three identical 5×5 cm^2 units will be stacked vertically and will be placed outside the vacuum chamber. If necessary, the calorimeters can be protected against soft radiation by placing an absorber in front of them and by adequate shielding on the other sides. The energy resolution in this configuration is $\Delta E/E = 0.25/\sqrt{E(\mathrm{GeV})}$. A fourth (retractable) calorimeter module will be used in the beamline in order to locate the high-energy γ beam and while tuning the e-ω and γ-ω interaction points.

2.5 Backgrounds

Since we are looking for single tracks in the presence of a primary beam of 10^{10} electrons and since the beam is pulsed at the ps level special attention must be paid to all possible backgrounds.

(i) Synchrotron radiation from the primary beam: Note that the secondary beamline is at 0.4 mrad to the primary line. Thus over a 12-m path length, the offset is 5 mm and appropriate masks can be set to shield the secondary beamline. The synchrotron radiation from the 50-μrad soft bends has a critical energy

$$\omega_c = \frac{3}{2}\,\gamma^3(c/\rho) = 15 \text{ keV} \tag{16}$$

and therefore can be removed from the beam line with thin absorbers. For the hard x-rays, $k > 10k_c$, the absorber is not effective but the integrated rate is approximately 10^{-7} per beam electron, equal to the Compton rate. A small sweeping magnet downstream of the absorber (and of the scrapers) would be helpful in cleaning up the secondary beamline.

(ii) Beam-gas bremsstrahlung: For a pressure of 10^{-6} torr, assuming that the residual gas is primarily CO, and for an acceptance of 50 μrad for the secondary beamline, the differential scattering probability for bremsstrahlung along the 1-m straight section around IP1 is

$$dP/dE_\gamma = 10^{-12}/E_\gamma/\text{per beam electron} \tag{17}$$

Integrating from $E_\gamma = 100$ keV to 50 GeV we have $P \approx 10^{-11}$/electron, so that a vacuum of 10^{-6} torr should be adequate for the proposed electron-beam intensities.

(iii) Muons from the beam dump: We wish to keep this background at a level below 1 muon/cm^2-pulse. This implies a radiation level at the detector of less than 1 mR/hr with the beam operating at 10 Hz. The present shielding specifications are such as to bring the level to 0.05 mR/hr which should be adequate.

(iv) Muons from the beamline: We can estimate this rate assuming a 1% loss in the beam transport and 10^{-4} muons/electron; we further assume that the muons are distributed over an area of 4-m diameter. Thus for a primary beam of 10^{10}/pulse the background rate is 0.1 muons/cm^2-pulse.

(v) Soft background in the enclosure: While this background does not affect the pair spectrometer it gives a feeling for the radiation in the beam enclosure; the positron calorimeter will have to be adequately shielded against this radiation. The origin of the radiation is backstreaming from the beam dump, and the laser-beam interactions which degrade the primary electrons.
We assume 10^6 Compton scatters per pulse yielding 20-GeV electrons (on average) which interact in the beam pipe. Thus 2×10^7 GeV of energy is absorbed in electromagnetic cascades at small grazing angles. Assuming that this radiation thermalizes, yielding 1-keV x-rays for every MeV of energy we have a source of 2×10^{10} x-rays/pulse; the isotropic density at a distance of 10 m is 10^3/cm^2-pulse. This is consistent with observations in the Compton polarimeter line of the SLC; in that area a foot of lead shielding is necessary to allow the operation of single particle detectors.

3 Nonlinear Compton Scattering

Backscattering of a low-energy photon ω_0 from a high-energy electron beam results in an energetic gamma ray moving along the electron beam's direction [10]. The energy of the gamma ray is

$$\omega = \omega_0 \frac{4\gamma^2}{1 + 2\gamma^2(1-\cos\theta) + (2\gamma\omega_0/m)(1+\cos\theta)} \tag{18}$$

where $E_e = \gamma m$ is the electron energy and θ is the laboratory scattering angle, which is of order $1/\gamma$. It is convenient to introduce the dimensionless parameters [2]

$$x = 4\omega_0 E_e/m^2, \qquad y = \frac{\omega}{E_e} \le y_{max} = \frac{x}{1+x}. \tag{19}$$

The differential cross section is then given by

$$\frac{d\sigma}{dy} = \frac{2\pi r_0^2}{x}\left[(1-y) + \frac{1}{(1-y)} - \frac{4y}{x(1-y)} + \frac{4y^2}{x^2(1-y)^2}\right] \tag{20}$$

with $r_0 = e^2/m = 2.82 \times 10^{-13}$ cm the classical electron radius. For $x > 2$ the total cross section can be approximated by

$$\sigma_C = \frac{2\pi r_0^2}{x}\left(\ln x + \frac{1}{2}\right). \tag{21}$$

In intense fields, the above equations are modified because of multiphoton absorption and of the transverse mass of the electron. Thus the energy of the backscattered photon is

$$\omega = n\omega_0 \frac{4\gamma^2}{1 + 2\gamma^2(1-\cos\theta) + [2n\gamma\omega_0/m + \eta^2/2](1+\cos\theta)} \tag{22}$$

The differential cross section can be given in closed form when the incident photons are circularly polarized [23]:

$$\frac{d\sigma_n}{dy} = \frac{2\pi r_0^2}{x}\left\{-\frac{4}{\eta^2}J_n^2(z) + \left(2 + \frac{u^2}{1+u}\right)\left[J_{n-1}^2(z) + J_{n+1}^2(z) - 2J_n^2(z)\right]\right\} \tag{23}$$

In the above equations the index n labels the number of photons absorbed from the field of the laser and the parameters u, z are defined through

$$u \simeq \frac{y}{1-y}, \qquad y_{\max} = \frac{nx}{1+\eta^2+nx}, \qquad z = \eta\sqrt{1+\eta^2}\,\frac{2}{x}\sqrt{u\left(\frac{nx}{1+\eta^2} - u\right)}. \tag{24}$$

In Fig. 7 we show the differential cross section for

$$\begin{aligned} E_e = \gamma m &= 50 \text{ GeV} \\ \omega_0 &= 1.17 \text{ eV } (\lambda = 1{,}054 \text{ nm}) \\ \eta &= 0.4 \end{aligned}$$

Numerically

$$\eta^2 = \left(\frac{eE}{m\omega c}\right)^2 = 0.4\left[\frac{I}{10^{18}\text{ W/cm}^2}\right]\left[\frac{\lambda}{1.054\,\mu\text{m}}\right]^2 \tag{25}$$

We take the energy in the laser pulse to be $\mathcal{E} = 0.12$ J and the width $\Delta t = 1.2$ ps. The pulse is brought to a focus with radius $R = 2.8\ \lambda$, to yield a flux $I = 4 \times 10^{17}$ W/cm^2, which results in $\eta = 0.4$. These parameters are conservative and have been achieved in the laboratory [18]. The corresponding photon density at the focal point is

$$N_\omega/\text{cm}^2 = I\Delta t/\omega_0 = 2.6 \times 10^{24}\,\text{photons/cm}^2$$

[This equals the electron density in a 1-cm-thick sheet of lead.]

The laser pulse is brought into collision with the electron beam at an angle $\Delta = 12^\circ$ as discussed in Sec. 2.5. For the electron beam we assume the parameters discussed in Sec. 2.2. The rate of backscattered photons has been calculated by convoluting the two beam distributions with the cross section given by Eq. (23). We find that

$$N_\gamma \sim 10^3/\text{interaction}$$

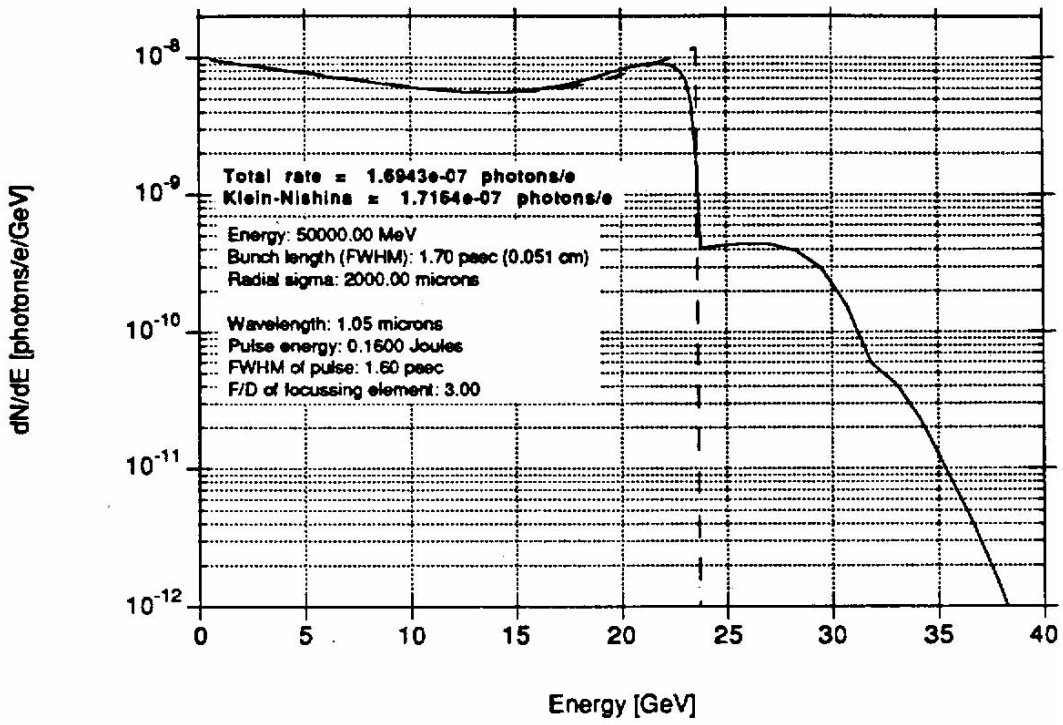

Figure 7: Differential cross section for multiphoton scattering of a $\lambda = 1,054$ nm laser pulse from 50-GeV electrons.

with energy $E_\gamma > 6$ GeV. The photons are contained within an angle $\theta < \sqrt{2}/\gamma$ which includes the electron beam divergence and the scattering angle. The photons are transported to the beam spectrometer, located 100 m downstream. Since the typical production angle is 10^{-5} rad, the γ-ray beam divergence is small and a 2-inch-diameter vacuum pipe is more than adequate; provided the alignment is maintained.

The pair spectrometer was discussed in Sec. 2.3. A small fraction ($\sim$0.5%) of the incident γ's is converted in the entrance CCD and subsequently analyzed in the spectrometer. We are interested only in the region $6 < E_\gamma < 30$ GeV and expect to be able to analyze up to three conversions per pulse. If the interaction rate is too high the electron beam will be defocused. We would like to accumulate 200 events in the third harmonic which implies collecting 50,000 γ's. This data can be obtained in one day's running and is sufficient to show the shift of the end point of the first harmonic due to the electron's transverse mass effect.

This experiment will be among the first observations of multiphoton Compton scattering. By varying η the effect of laser beam intensity on the cross section can be studied. It will also provide us with the necessary experience on the mutual alignment of the beams and of their time-synchronization. The information on the yield and spectral quality of the backscattered photons is, of course, necessary for refining the γ-γ scattering experimental setup.

4 Beamstrahlung

Of primary interest in the design of future linear colliders is the degradation of the primary beams due to beamstrahlung. In addition, low-energy e^+e^- pairs produced by beamstrahlung can result in serious background in the detector. Our experimental set-up makes it possible to test some of these predictions because the electrons passing through the laser focus see a near-critical field. In the multiphoton Compton experiment, the intensity parameter was set at $\eta = 0.4$ which corresponded to $\Upsilon = 0.1$. [Note that $\Upsilon = \eta x/4$.] For the beamstrahlung we expect to work at $\Upsilon = 0.3$; this can be achieved by increasing the energy in the laser pulse, while also focusing more tightly, reaching peak values of $\eta = 1.2$.

We first consider pair production in intense fields. We follow Chen and Telnov [24]. The number of pairs per electron

$$n_p = \frac{4\sqrt{3}}{25\pi} \left[\frac{\alpha\sigma_z}{\gamma\lambda\!\!\!^{-}_c}\,\Upsilon\right]^2 \Xi(\Upsilon) \qquad \Upsilon \ll 1 \tag{26}$$

σ_z is the length of the laser focal region, and the function $\Xi(\Upsilon)$ decreases exponentially for $\Upsilon < 1$. For $\Upsilon = 0.3$, $\gamma = 10^5$ and $\sigma_z = z_0 = 30\ \mu$m

$$n_p = 2.3 \times 10^{-7},$$

Eq. (26) is obtained from the rescattering of real photons, and therefore depends quadratically on σ_z since it describes a two-step process. The contribution of virtual photons (tridents) is very much suppressed for $\Upsilon \ll 10$. As discussed in Sec. 2.3 we will measure the positron energy spectrum for $5 < P_+ < 25$ GeV/c. Altering the focal properties of the laser beam decreases Υ which leads to a drastic reduction in the pair rate because of the dependence on $\Xi(\Upsilon)$; this is not the case for γ-emission.

To estimate the γ-emission rate we use the expression for the fractional energy loss of an electron in a high field as given by Chen and Yokoya [8]

$$\epsilon = \frac{I}{E_e} = \frac{\sqrt{\pi}}{3}\,\frac{\alpha\sigma_z}{\lambda\!\!\!^{-}_c\gamma}\,\Upsilon^2 \qquad \Upsilon \ll 1 \quad . \tag{27}$$

Using $\sigma_z = z_0 = 30\ \mu$m and $\Upsilon = 0.3$ we find $\epsilon = 0.1$; thus the electrons loose a significant fraction of their energy. A measure of this energy loss are the high energy γ's emitted outside the single photon cone of 10 μrad. The spectrometer acceptance extends to 100 μrad and we propose to measure the γ-spectrum in the energy range $6 < E_\gamma < 30$ GeV. This corresponds to a range in transverse momentum $0.06 < P_\perp < 3$ MeV/c which is typical of these processes where the only transverse kick comes from the electron mass.

The dependence of Eq. (27) on σ_z and Υ can be checked by decreasing the laser intensity. It is interesting to note that to first order Eq. (27) is independent of the f-number (f/D) of the laser focusing mirror.

5 The Multiphoton Breit-Wheeler Process

We wish to investigate pair production by real photons

$$n\omega_0 + \omega \rightarrow e^+e^- \tag{28}$$

As mentioned in the introduction we use a UV pulse to create the photon beam which has the spectrum shown in Fig. 3. The beam is brought into collision with the remainder of the UV pulse which is now focused to high intensity ($\eta = 1.2$) to make multiphoton absorption probable.

Pair creation by n laser photons is the cross-channel process from nonlinear Compton scattering, and for circular polarization of both the laser photons and the high-energy photon is given in analogy to Eq. (23) by [23]

$$\frac{d\sigma_n}{dy} = \frac{2\pi r_0^2}{x}\left\{\frac{4}{\eta^2}J_n(z) + (u-2)\left[J_{n-1}^2(z) + J_{n+1}^2(z) - 2J_n^2(z)\right]\right\} \tag{29}$$

where (for $n\omega_0 \ll \omega$)

$$x = \frac{4\omega_0\omega}{m^2}, \qquad y = \frac{E_e}{\omega}, \qquad y_{\max,\min} = \frac{1}{2} \pm \sqrt{\frac{1}{4} - \frac{1+\eta^2}{nx}}, \qquad u = \frac{1}{y(1-y)}, \tag{30}$$

and z is defined as before. The cross section exists only for those values of n such that $y_{\max}$ is real.

The cross section for reaction (28) for $\eta = 0.4$ and $\omega_0 = 3.5$ eV, is shown in Fig. 8 as a function of the energy of the γ. The thresholds for pair production via n laser photons are given by

$$E_n = \frac{m^2(1+\eta^2)}{n\omega_0}. \tag{31}$$

The thresholds for $n = 1$ at 86.2 GeV, $n = 2$ at 43.1 GeV, and $n = 3$ at 28.7 GeV are visible in the Figure. For γ's from Compton backscatter from a 50-GeV electron beam, the maximum energy is 36.5 GeV at which energy three laser photons are required for pair production. The cross section reaches a maximum of 1.6×10^{-25} cm^2 for $E_\gamma \approx 155$ GeV. At this energy the pair-production cross section is almost the same as the Compton cross section, so pair production would be very prominent.

Figure 9 illustrates the nonlinear dependence of the pair-production cross section on the laser field strength. It varies as η^4 for weak fields, but saturates at $\eta \approx 1.5$.

Figure 10 shows the differential cross section for pair production as a function of the lab energy of the electron or positron. For the parameters considered, the electrons are nonrelativistic in the pair rest frame, so the lab energies do not extend down to zero or up to the incident-γ energy. The kink in the curve corresponding to $\eta = 0.4$ is at the transition between dominance by three and by four laser photons.

Since reaction (28) has not been observed with real photons it is of interest to confirm the cross section and this is the goal of the present measurement. The pairs are moving in the forward direction and have a very small opening angle, but they are accompanied by an intense high energy γ-flux. Thus it is impractical to measure their angle before they enter the spectrometer magnet. Once the pair is dispersed by the magnet, the e^+ and e^- trajectories are reconstructed and are traced (through the magnet) back to the interaction point; this allows the determination of the momenta and of the opening angle. The track segments in the non-bending (vertical) plane serve to remove ambiguities and reject background.

The mass resolution is evaluated from

$$M^2 \simeq 4m^2 + P_+P_-\theta^2 \tag{32}$$

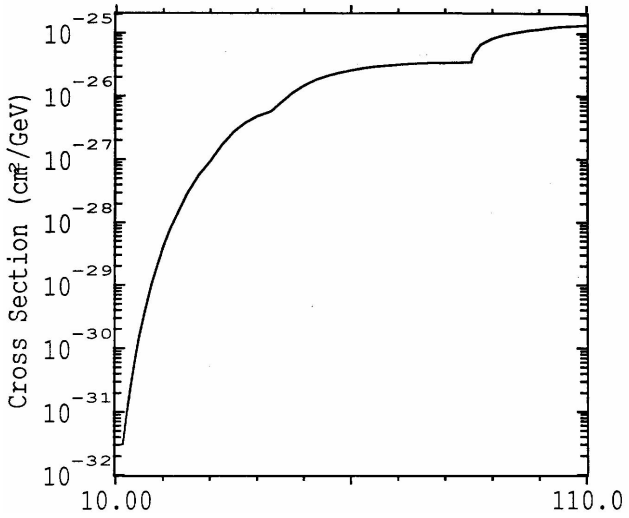

Figure 8: Total cross section for pair production when high-energy photons are incident on a $\lambda = 350$ nm laser pulse with field strength $\eta = 0.4$. The thresholds for production via 1, 2, and 3 laser photons are visible at 86.2, 43.1, and 28.7 GeV, respectively.

with θ the opening angle and P_+, P_- the positron and electron momenta. For symmetric decays, $P_+ \sim P_- \sim 20$ GeV so that $\theta \sim 3 \times 10^{-5}$ at $M = 1.2$ MeV. Since

$$\sigma_M = \frac{M^2 - 4m^2}{2M} \sqrt{2\left(\frac{\sigma_P}{P}\right)^2 + \left(\frac{\sigma_\theta}{\theta}\right)^2} \tag{33}$$

we wish to measure θ and P_+, P_- to $\sim 2\%$ accuracy. This requires $\sigma_\theta \sim 6 \times 10^{-7}$ which corresponds to a precision in the measurement of the separation of the two track segments in the center of the analyzing magnet, (located at 100 m from IP1) $\Delta x = 60$ μm. As discussed in Sec. 2.3 the accuracy in the projection of the track segment is dominated by multiple scattering and ranges from 32 to 160 μm from the highest (30 GeV/c) to the lowest (6 GeV/c) momentum: For the charged-particle momenta the 5-μm spatial resolution of the CCD allows a determination $\Delta P/P \sim 0.6\%$ including-multiple scattering effects.

As we are very near threshold for pair production in the proposed experiment, the rate for this is slower than for Compton scattering. Given an effective cross section for 3-photon absorption

$$\sigma_{(3\omega_0+\omega' \to e^+e^-)} \simeq 10^{-27}\,\mathrm{cm}^2$$

and a photon density of $10^{24}/\mathrm{cm}^2$ the pair-production probability is 10^{-3}. The high-energy-photon flux is estimated at 10^4/pulse. Depending on the focal properties of the electron beam, 10% of these high-energy photons will cross through the laser focus. We assume another factor of 10 for selection of symmetric pairs and detection efficiency in the presence of the high-energy photon beam. Thus we expect 1 pair/10 pulses or 10^4 pairs in one day, which is more than sufficient to establish the cross section and study the low end of the mass spectrum.

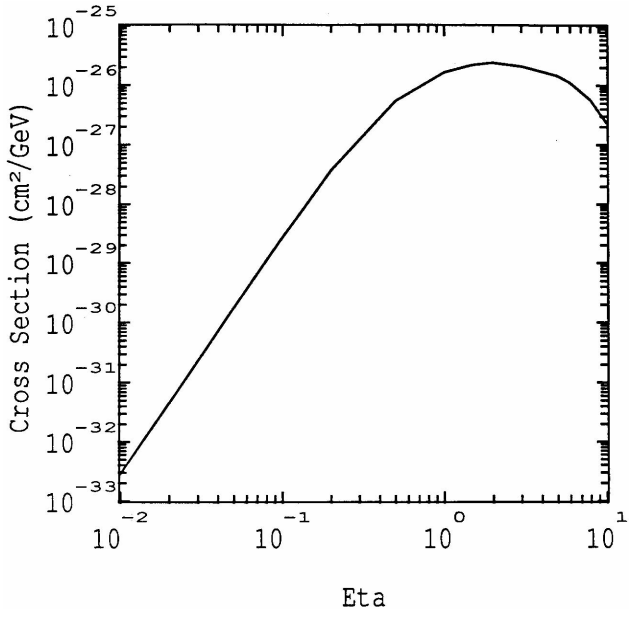

Figure 9: Total cross section for pair production when 36.5-GeV photons are incident on a $\lambda = 350$ nm laser pulse of field strength η.

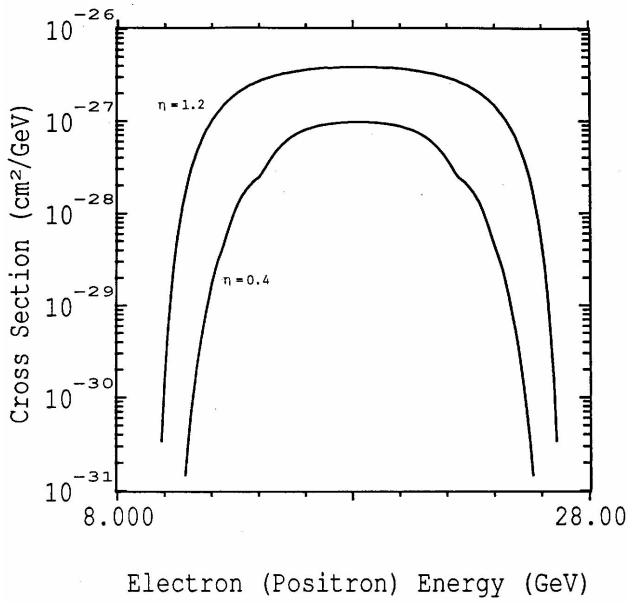

Figure 10: Differential cross-section *vs.* electron (or positron) energy for pair production when 36.5-GeV photons are incident on a $\lambda = 350$ nm laser pulse. Lower curve: intensity parameter $\eta = 0.4$; upper curve: intensity parameter $\eta = 1.2$.

6 The e^+e^- Mass Spectrum in High Fields

In Fig. 11 we show the effective mass of the e^+e^- pairs as observed at the Darmstadt experiments [5]. As already mentioned, an explanation for these peaks is that they are due to a strong-field QED process.

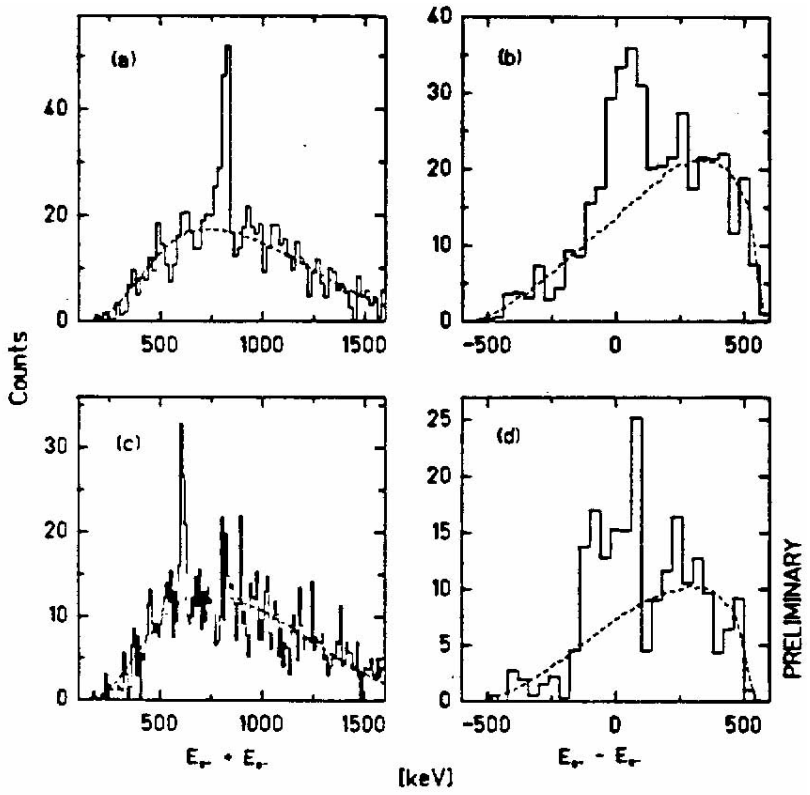

Figure 11: Results of a preliminary analysis of U + Th collisions near 5.87 MeV/c [5]. The $(E_{e^+} + E_{e^-})$ projections are for two subsets of data gated on beam energy, heavy-ion scattering angle and e^+ or e^- TOF chosen to enhance the prominent sum lines at $\sim$ 810 keV and $\sim$ 620 keV, respectively.

Another experiment involving strong-field QED is in progress at CERN [25]. It involves 100-GeV tagged γ's incident along the $\langle 110 \rangle$ direction of a 400-μm-thick germanium crystal. The mass spectrum of the produced e^+e^- pairs is measured in a simple spectrometer located 80 m downstream from the target. When the e^+e^- vertex is in the target the events are referred to as "short lifetime" and the preliminary spectrum presented at Moriond is shown in Fig. 12. Since then further analysis has removed the structure at 2.2 MeV/c^2. However the experimenters still observe 47 events with "long lifetime", defined to have a decay vertex further than 8 m from the target [25]. Among these events are 13 that cluster near an invariant mass of 3.5 MeV/c^2 and lifetime 3×10^{-12} s, while only 4 would be expected there on comparison with the rest of the spectrum. If these phenomena are indeed related to

strong-field QED they should be reproduced in the proposed experiment.

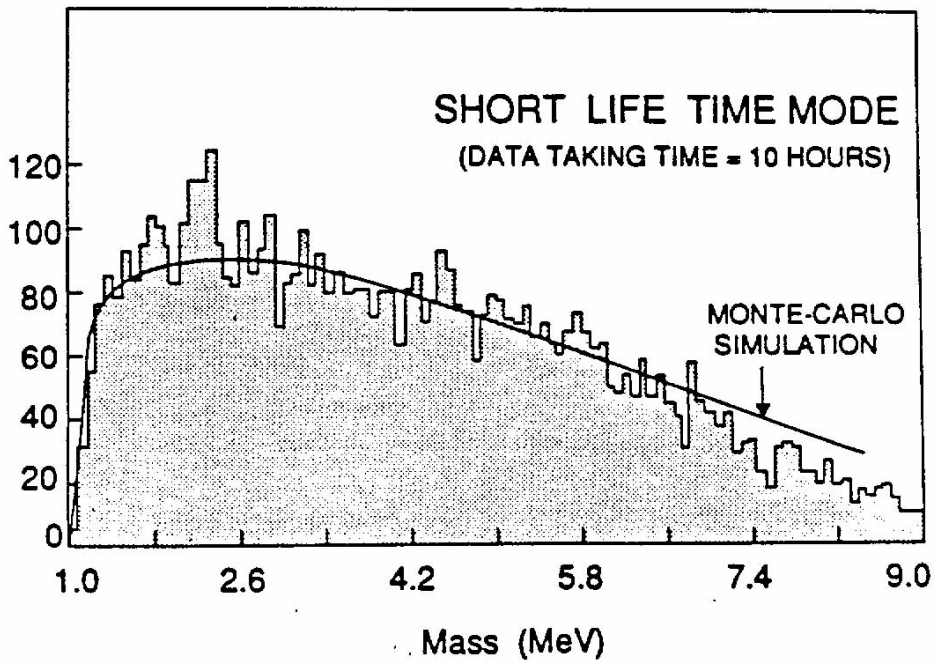

Figure 12: Preliminary results from high-energy-γ channeling in crystals. From ref. [24].

We can extend our proposed studies of pair-production to explore the possibility of structure in the invariant-mass spectrum. The apparatus and layout are the same as in the previous measurement of the low end part of the spectrum. The principal difference is that to reach high masses (up to 2 MeV/c^2) we must have sufficient probability for the absorption of $n \gtrsim 8$ photons. Thus the intensity parameter of the laser beam will have to be set at $\eta \gtrsim 1$.

Figure 13 shows that rate of pair production per 36.5-GeV photon as a function of the electron (or positron) lab energy for seven laser-pulse energies: 0.01, 0.03, 0.1, 0.3, 1, 3, and 10 Joules. In all cases a lens with $f/D = 3$ is assumed, and we suppose that the high-energy photon beam has a radial σ of 60 μm as discussed in Sec. 2 and Appendix A. The spectra are narrower than the beam energy as the production is close to threshold and the electrons are nonrelativistic in the pair rest frame.

The invariant mass of the pair, when it is still in the laser field, is given by

$$\overline{M} = \sqrt{s} = 2\sqrt{n\omega_0\omega} = 0.75\sqrt{n}\ \text{MeV}/c. \tag{34}$$

That is, a line spectrum of pair masses is produced, depending on the number n of laser photons absorbed. The pair-production rate as a function of the number of laser photons absorbed is shown in Fig. 14 for seven laser-pulse energies.

A complication arises in interpreting the mass spectrum because the e^+e^- are produced in a strong field where the effective mass of the electrons is $\overline{m} = m\sqrt{1+\eta^2}$, and its 4-vector

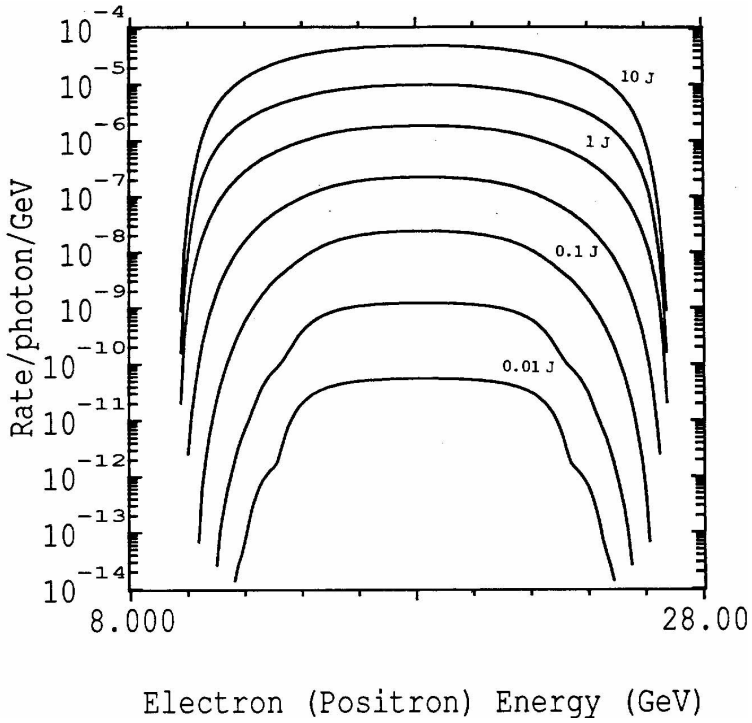

Figure 13: The calculated rate of pair production in collisions of a 36.5-GeV photon with a laser beam of 3.5-eV photons, as a function of the energy of the produced electron (or positron). The laser is focused in a lens of $f/D = 3$, and the high-energy photon beam has a radial σ of 60 μm. The seven curves are, from bottom to top, for 0.01, 0.3, 0.1, 0.3, 1, 3, and 10 Joule laser-pulse energies. Corresponding to these are $\eta_{\max} = 0.21$ 0.37, 0.67, 1.16, 2.12, 3.68, 6.71, and $\Upsilon_{\max} = 0.11$, 0.18, 0.33, 0.58, 1.05, 1.82, and 3.32, respectively.

is modified to be

$$\overline{p} = p + \kappa\omega_0, \qquad \kappa = \frac{m^2\eta^2}{2(\overline{p}\cdot\omega_0)} \tag{35}$$

with ω_0 the laser-photon 4-vector. As a result the effective mass of the pair in the strong field is

$$\overline{M}^2 = (\overline{p}_1 + \overline{p}_2)^2 \tag{36}$$

In case of symmetric production the invariant mass observed outside the laser beam is

$$M^2 = (p_1 + p_2)^2 = \overline{M}^2 - 4m^2\eta^2 \tag{37}$$

whereas for forward/backward production

$$M^2 = \overline{M}^2/(1+\eta^2) \tag{38}$$

If we write in general

$$\overline{M}^2 = 4m^2(1+\eta^2+\Delta) \quad . \tag{39}$$

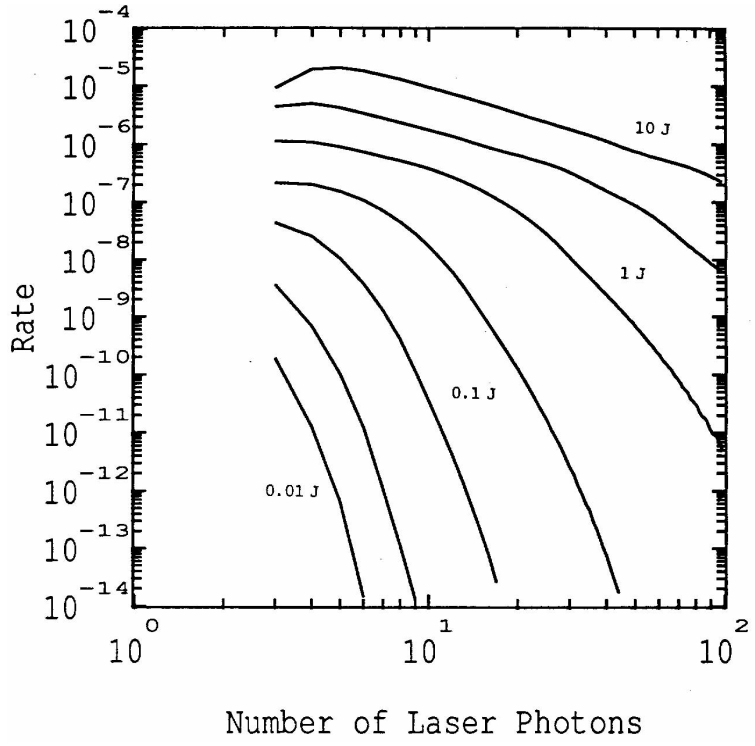

Figure 14: The calculated rate of pair production as a function of number of laser photons, for the conditions of Fig. 13.

Then the corresponding M^2 once the pair leaves the strong field will vary over the range

$$1 + \frac{\Delta}{1+\eta^2} \leq \frac{M^2}{4m^2} \leq 1 + \Delta. \tag{40}$$

In the limit of large η, the lower limit of the range is just $M = 2m$ no matter what the value of $\overline{M}$! If it appears that the physics requirement is for good mass resolution in $\overline{M}$ rather than M, it may be necessary to restrict the experiment to nearly symmetric decays. Experimental reality may force this requirement anyway, since one member of an asymmetric pair always lies closer to the unscattered beam than for a symmetric pair, and detection is simpler in the symmetric case. Figure 15 shows a calculation of the expected pair mass spectrum outside the laser beam.

Figure 11 shows the rate of pair production as a function of the pair mass as observed outside the high-field region, for seven laser-pulse energies. At very low laser field strengths the invariant mass is little affected by the laser, and the line spectrum can still be discerned. At large field strengths the intrinsic line spectrum will be smeared into a continuum. We see that laser-pulse energies of order 1 Joule would be advantageous to study pair masses near 2 MeV/c^2.

Departures from the QED prediction [23] might then arise in two ways. The intrinsic line spectrum might not be as expected, or the smearing of that line spectrum into the laboratory continuum might be altered. While a single run as proposed might be sufficient to reveal

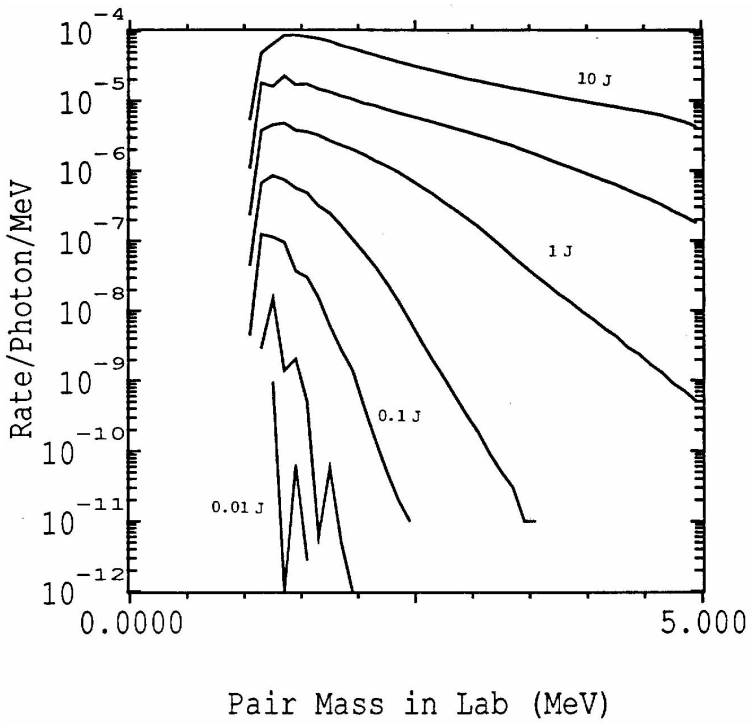

Figure 15: The calculated rate of pair production as a function of the pair mass as measured in the laboratory, for the conditions of Fig. 13. The intrinsic line spectrum is smeared into a continuum as the electrons leave the strong-field region.

the second effect, a scan of primary electron-beam energies would be required to explore the first effect.

Another potential loss of mass resolution is Compton scattering of the electron or positron before they leave the strong-field region of the laser beam. This effect increases as η^2 and a possible way to circumvent it is to use only events where the electron and positron energies add up to the beam energy.

If a laser pulse of one Joule is used, the total pair rate per high-energy photon is about 10^{-5} according to Fig. 9. We saw in Sec. 2 that if 0.16 Joule of laser light is used to create the high-energy photons then about 3×10^5 of these would be produced in a 9% energy bite. Then the total pair rate would exceed one per pulse, and the overlapping pairs could not be analyzed. The laser intensity at the first interaction point should be reduced to perhaps 10 mJoule to keep the pair rate to 1/3 per pulse. With 1-Hz laser operation some 25,000 pairs could be collected per day. Even if the laser pulse energy is restricted to 0.3 J at the γ-ω interaction point, the event rate is sufficient to carry out the measurement in a few days.

7 The Laser System

We have built a laser system capable of delivering 1-Joule pulses of infrared light at $\lambda = 1.05\,\mu$m with the system presently operating at the 300-mJ level [26,27]. A laser pulse from a mode-locked oscillator is frequency chirped, temporally expanded in a fiber, and further stretched in time by an expansion grating pair. The longer pulse allows more energy to be extracted from the subsequent amplifier system than would be by a short pulse. After amplification, the pulse is compressed by a grating pair to picosecond or subpicosecond duration [28]. There is a resulting increase in power equal to the chirp ratio, the stretched-pulse duration divided by the compressed-pulse duration. The chirping in the fiber, the compression and expansion grating pairs, and the chirp ratio are well described in the literature [29-32].

A schematic diagram of the present CPA laser system is shown in Fig. 16. It consists of three parts: the pulse-preparation stage, the amplifier chain, and the compression stage. The top part of Fig. 16 shows the pulse-preparation stage. A cw-pumped mode-locked Nd:YLF oscillator generates a 100-MHz train of 50-ps pulses at a wavelength of 10530 A. The pulses are coupled into a 0.8-km single-mode optical fiber with a 9-μm core and then sent through a pair of expansion gratings. Due to self-phase modulation and group-velocity dispersion in the fiber, and further dispersion by the expansion grating pair, the pulses are chirped to approximately 300 ps across a 37-A bandwidth. A single nanoJoule-energy pulse is selected by a Pockels cell and seeded into a Q-switched, end-mirror-dumped regenerative amplifier. The amplifier uses a 7-mm-diameter phosphate Nd:glass rod (Kigre Q98). (A carefully designed regenerative amplifier not only amplifies the laser pulse but also shapes the laser spectrum [33]. For this reason, the regenerative amplifier is considered part of the pulse-preparation stage.) A 1-mJ pulse is selected from the pulse train, which is transmitted through the 50% reflective end mirror in the regenerative amplifier. The spatial profile of the beam is cleaned with an air spatial filter. An attenuator consisting of a half-wave plate between two polarizers is used to control the energy input to the amplifier chain. The cw autocorrelator monitors compressed pulses before amplification. The compression is done with a small compression grating pair, which is matched to the compression gratings after the amplifier chain.

The amplifier chain consists of a double-pass 9-mm-diameter amplifier (Kigre Q-98, 235 mm long), and a single-pass 16-mm-diameter amplifier (Hoya LHG-8, 360 mm long). A single-pass 30-mm-diameter amplifier (Hoya LHG-8, 360 mm long) will be added when compression gratings with a higher damage threshold are installed. One Pockels cell after the 9-mm amplifier further isolates the pulse and suppresses any feedback pulse, which may result from reflections off optical elements. An additional attenuator increases the system's dynamic range to 10^6. A vacuum spatial filter after each amplifier is used to upcollimate, image relay, and spatially filter the pulse. The energy of the chirped pulse after the 16-mm amplifier can be as high as one Joule with a repetition rate of 1 shot per 70 sec (limited by the thermal lensing in the 16-mm amplifier rod).

The compression stage consists of two 1700-line/mm gold-coated holographic gratings, with dimensions 80×110 mm. The gratings are used in the near-Littrow, double-pass configuration with a separation distance of 164 cm. The laser pulse is compressed to 1.6 ps with a bandwidth of 13.5 A when no saturable absorber is used. The laser beam has a 36-mm diameter limiting the maximum energy to 300 mJ currently, due to the damage threshold of

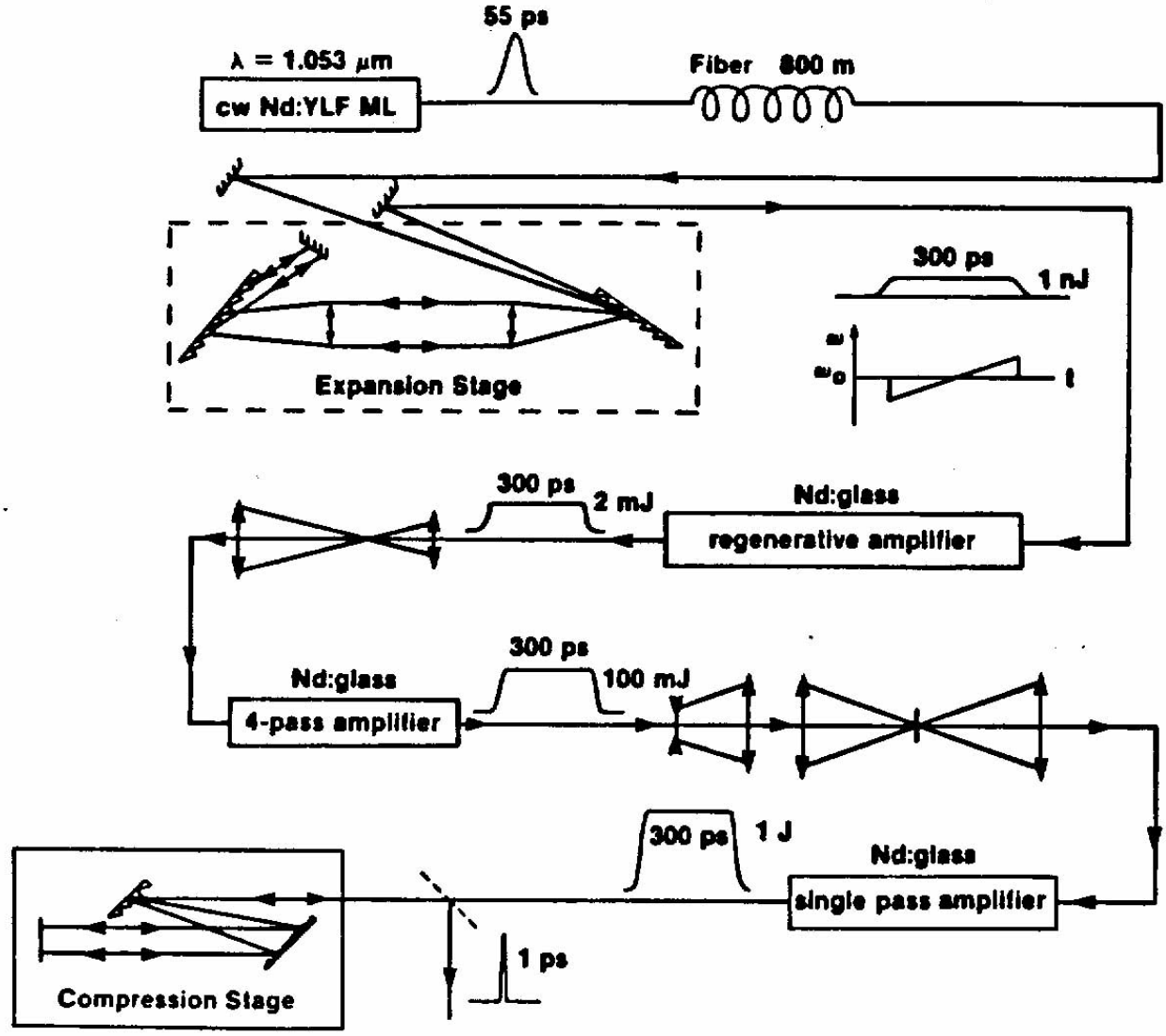

Figure 16: Chirped-pulse amplification and compression. A pulse from the mode-locked oscillator is chirped in a fiber and amplified before being compressed to a pulselength of less than 2 psec.

the compression gratings. An autocorrelator and an energy meter are used to measure the final pulse width and pulse energy after compression. A saturable absorber has been used to clean up the pulse wings and produce a 0.9-ps Gaussian laser pulse when this is necessary. The autocorrelation trace of the pulse is shown in Fig. 17.

With the compression gratings currently in the system, we are limited to laser pulse energies of ~ 100 mJ to avoid damage. With new 16×25 cm gratings and with the addition of an upcollimator, we will be able to take advantage of our full amplification capabilities, and produce laser energies in excess of 1 J and intensities significantly in excess of 10^{18} W/cm^2.

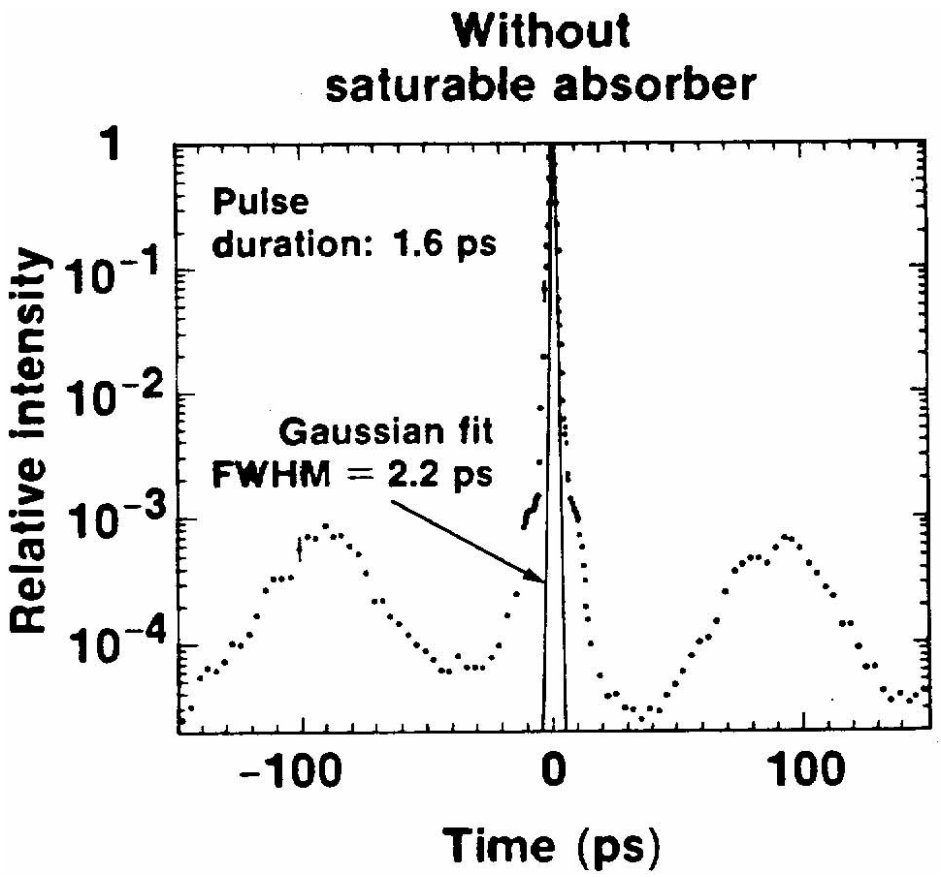

Figure 17: Autocorrelation of the compressed pulse. Assuming a gaussian profile, this measurement corresponds to a pulsewidth of 1.6 picoseconds. Note the logarithmic scale.

The limitation of the present system is its repetition rate. However, a large-aperture, high-gain, slab-geometry, Nd:glass amplifier has been designed, constructed, characterized, and routinely operated at the University of Rochester. This amplifier was specifically designed to provide high-energy (∼3 J), 0.3-1.0-ns pulses at medium repetition rate (2 Hz) with the superior beam quality (both phase and polarization) required for efficient frequency *tripling*. These requirements are an excellent match to the chirped-pulse amplification stage of our present laser system. This amplifier has been in operation for over one year with in excess of 200,000 shots delivered. We propose to duplicate this proven design, using it to replace the repetition-rate-limiting final amplifier stages of the current laser system, and to operate at 1 Hz. The cost in providing this system is estimated at $100,000.

The final step that must be addressed is the generation of UV pulses by upconverting the IR. We have decided to triple the IR pulse because of the high efficiency (80%) [34] for this process as demonstrated at the University of Rochester Laboratory for Laser Energetics for nanosecond pulses [35]. We have performed experiments [36] using picosecond pulses and confirm the predictions of Wang and Dragila [37], having achieved 75% efficiency for

frequency doubling of a 1-ps IR pulse. An alternative is to triple the pulse frequency before compression; this is possible by angularly dispersing the beam in the crystal and then recollimating it. In this case UV gratings, which have recently become commercially available, must be used.

8 Appendix A: The e-ω and γ-ω Interaction Regions

We examine here in greater detail the optimum focusing of the electron and laser beams in the Breit-Wheeler experiment. The discussion includes the emittance of the electron beam as well as the scattering angle of the high-energy γ's with respect to the electrons.

The laser spot at the second (γ-ω) interaction point must be only a few wavelengths across to maintain the highest possible electric field. If a high-energy γ is produced by a Compton scatter in the first (e-ω) interaction at a radius r_1 from the beam axis, it must have lab angle $-r_1/L$ to arrive usefully on axis at the second interaction point, which is distance L downstream. The lab angle is compounded of the scattering angle θ, and the slope r' of the incident electron. To arrive at $r = 0$ at the second interaction point, a γ should have scattering angle $\theta = -r_1/L - r' = -(r_1 + r'L)/L = -r_2/L$, where r_2 is the position of the electron at the second interaction point if it had not scattered. Thus the electron beam size at the second interaction point should be

$$\sigma_{r_2} = L\Delta\theta \approx 60\ \mu\text{m}$$

when $L = 10$m, and $\Delta\theta = 6\ \mu$rad is the desired acceptance in Compton scattering angle as considered in Sec. 2 above.

The electron beam is, in general, focused at a distance z upstream of the second interaction point. If the beam has emittance ϵ and the focusing system is described by the strength $\beta^\star$, we have

$$\sigma_{r_2}^2 = \epsilon\beta^\star\left(1 + \frac{z^2}{\beta^{\star 2}}\right).$$

The electron beam size at the first interaction point, distance L upstream, is related by

$$\sigma_{r_1}^2 = \epsilon\beta^\star\left(1 + \frac{(L-z)^2}{\beta^{\star 2}}\right).$$

For given ϵ and L, both $\beta^\star$ and z are to be optimized.

From Eq. (14) for the luminosity of the Breit-Wheeler experiment, we see that we should minimize the product of the area of the electron-beam spot at the first interaction point and the area of the high-energy photon beam at the second interaction point. The latter area is larger than that of the electron beam there due to Compton scattering. We can write

$$A_{\gamma_2} = \pi(\sigma_{r_2}^2 + \theta(E)^2),$$

where θ is the Compton scattering angle for γ's of energy E. For $E = E_{\max}$, $\theta = 0$; while for $E = E_{\min}$ given by Eq. (12), $\theta = \Delta\theta = \sigma_{r_2}/L$ by definition. In any case, the size of the γ beam at the second interaction point is linked to the size of the electron beam there, and not directly to the size of the electron beam at the first interaction point. So once the size of the electron beam at the second interaction point is fixed, the luminosity is a minimum when the electron spot at the first interaction point is also a minimum.

To effect this minimization we use the method of Lagrange multipliers, forming the function

$$f(\beta^\star, z) = \sigma_{r_1}^2 + \lambda\sigma_{r_2}^2$$

where λ is the multiplier. The minimum of f is at

$$\beta^\star = \frac{L\sqrt{\lambda}}{1+\lambda}, \qquad z = \frac{L}{1+\lambda},$$

and the constraint that $\sigma_{r_2} = L\Delta\theta$ implies that

$$\lambda = \frac{\epsilon^2}{L^2\Delta\theta^4}.$$

The optimum size of the electron beam at the first interaction point is then

$$\sigma_{r_1} = \frac{\epsilon}{\Delta\theta}.$$

For our standard example that

$$\epsilon = 3 \times 10^{-10} \text{ m-rad}, \qquad L = 10 \text{ m}, \qquad \Delta\theta = 6 \times 10^{-6},$$

we then have

$$\sigma_{r_1} = 50 \ \mu\text{m}, \qquad \sigma_{r_2} = 60 \ \mu\text{m}, \qquad \lambda = 0.7, \qquad z = 5.9 \text{ m}, \qquad \beta^\star = 4.9 \text{ m}.$$

The corresponding angular divergence of the electron beam is

$$\sigma_\theta = \sqrt{\epsilon/\beta^\star} = \Delta\theta\sqrt{1 + (\epsilon/L\Delta\theta)^2} \approx \Delta\theta = 6 \times 10^{-6}.$$

To obtain high-energy photons of energies down to $E_{\min}$, the laser spot size at the first interaction point should be of size σ_{r_1} also.

9 Appendix B: Synchrotron Radiation

Synchrotron radiation is a potentially severe background in the proposed experiments. Perhaps the best way to suppress it will be a thin tungsten foil placed in the backscattered photon beam between the last and next-to-last dump magnets. We could afford a foil as thick as several tenths of a radiation length, as the final dump magnet would sweep out both hard and soft electrons prior to the pair spectrometer, and prior to the gamma-laser interaction point. Thus this solution is equally effective for the Compton experiment and for the Breit-Wheeler experiment.

We sketch some formalism to judge the magnitude of the problem. The total (classical) radiation rate is obtained from the Larmor formula:

$$\frac{dU}{dt} = \frac{2}{3}\frac{e^2 a^{\star 2}}{c^3} = \frac{2}{3}\frac{e^2\gamma^4 c}{\rho^2},$$

where $a^\star$ is the acceleration in the electrons rest frame, and ρ is the radius of curvature. We have used $a_{\text{lab}} = v^2/\rho \approx c^2/\rho$, and $a^\star = \gamma^2 a_{\text{lab}}$ noting that the acceleration is transverse, so the transformation involves two powers of the time dilation.

The frequency spectrum is roughly exponential:

$$\frac{dU}{d\omega dt} \approx \frac{e^{-\omega/\omega_C}}{\omega_C}\frac{dU}{dt} = \frac{4}{9}\frac{\gamma e^2}{\rho}e^{-\omega/\omega_C},$$

where the critical frequency is

$$\omega_C = \frac{3}{2}\gamma^3\omega_0 \approx \frac{3}{2}\frac{\gamma^3 c}{\rho}.$$

The spectrum falls to zero at low frequencies as $\sqrt{\omega}$, but the exponential approximation is valid for $\omega > \omega_C/3$ [38, 2]. See the end of this section for a derivation of the high-frequency behavior.

If our apparatus is sensitive to radiation emitted over an angular interval $\Delta\theta$, then the corresponding time interval is $\Delta t = \rho\Delta\theta/c$. Introducing $L = \rho\Delta\theta$ as the path length in the magnetic field over which bend $\Delta\theta$ occurs, we can write the critical energy as

$$E_C = \hbar\omega_C = \frac{3}{2}\frac{\gamma^3}{\alpha}\frac{r_e}{L}\Delta\theta mc^2.$$

Introducing photon energy $E = \hbar\omega$, the number of photons emitted into our angular acceptance is then

$$dN = \frac{4}{9}\gamma\alpha\Delta\theta e^{-E/E_C}\frac{dE}{E}.$$

A rough estimate of the number of photons emitted in an interval $dE/E = 1$ around the critical energy is just

$$N \approx \gamma\alpha\Delta\theta,$$

independent of the value of the critical energy.

Some numerical examples. The angular acceptance of the pair spectrometer will be about ± 5 mm at 100 m, so $\Delta\theta \approx 10^{-4}$. Of course, $\gamma \approx 10^5$ at SLAC. Then the number of synchrotron-radiation photons with energy near the critical energy is about

$$N = 0.1 \text{ per electron.}$$

If we use one of the permanent dump magnets to provide a bend of 500 μrad in one meter, we get a bend of $\Delta\theta$ in only 20 cm. Hence for this we have

$$E_C = 147 \text{ keV}.$$

Suppose we reduce the strength of the permanent magnets to provide a bend of only 50 μrad over 1 meter. This reduces the critical energy to about 15 keV.

If we can obtain extra space along the beamline to use the Russian magnets for both soft bends, then their length of 2.5 m implies a critical energy of 6 keV for 50-μrad bends each.

Suppose we put a tungsten absorber of thickness T_W just before the last dump magnet. The x-ray absorption length λ_W in tungsten is calculated from fits, including K, L, M, and N-edges, published in UCRL-50174 [39]. The number of x-rays emerging from this absorber is then, of course, $\exp(-T_W/\lambda_W)$.

Our silicon detectors will have an effective thickness for x-ray absorption of about 100 μm, equivalent to about $T_{Si} = 23$ mg/cm^2. The absorption length for x-rays in silicon is also

taken from UCRL-50174. Hence if N_e is the number of electrons in a pulse, the number of x-rays that penetrate the tungsten absorber and are then absorbed in the silicon detector to cause extra hits is

$$N = \frac{4}{9} N_e \gamma \alpha \Delta\theta \int_{E_C/3}^{\infty} e^{-E/E_C} e^{-T_W/\lambda_W} \frac{T_{Si}}{\lambda_{Si}} \frac{dE}{E}.$$

We desire $N \leq 1$.

The integral has been evaluated numerically, using the stated approximations for the x-ray absorption lengths. We find that for $N_e = 10^{10}$ we could achieve the condition $N = 1$ for a critical energy of 6 keV by using a tungsten absorber of 0.95 g/cm^2, corresponding to 14% of a radiation length. For a critical energy of 15 keV we would need a tungsten absorber of 2.9 g/cm^2, corresponding to 42% of a radiation length. Recall that a pair-creation length for high-energy photons is 9/7 of a radiation length. In all cases the most troublesome x-ray energy is 9-10 times the critical energy, for which a thin absorber causes very little attenuation of the flux. Fortunately there are not too many x-rays so far above the critical energy, and they do not interact greatly with the silicon detector.

The situation varies slightly with other absorbers. Again using x-ray absorption fits from UCRL-50174, we find that for a critical energy of 6 keV, 0.75 g/cm^2 (11% rad. length) of lead is sufficient, and 0.55 g/cm^2 (9% rad. length) of uranium would do. For 15-keV critical energy we would need 3.2 g/cm^2 (50% rad. length) of lead, or 3.3 g/cm^2 (55% rad. length) of uranium. The different Z-dependence for different critical energies arises because high-Z materials have a K-edge near 100 keV.

It appears that we could suppress synchrotron radiation to an acceptable level by use of tungsten absorbers at 15-keV critical energy, corresponding to use of the 1-m-long permanent dump magnets for the 50-μrad soft bends. The price would be a 30% attenuation of the flux of high-energy backscattered photons.

Frequency Spectrum of Synchrotron Radiation

We will use Feynman's expression for the radiation field of an accelerated charge [40] to calculate the frequency spectrum of synchrotron radiation. Supposedly it was this problem that led him to invent the formalism.

A charge e moves in a circle of radius r about the origin in the x-y plane:

$$x = \rho \sin \omega_0 t,$$

$$y = \rho \cos \omega_0 t.$$

We observe the radiation at $(x, y) = (r_0, 0)$ where $r_0 \gg \rho$. Feynman tells us that the radiation field has y-component

$$E_y \approx -\frac{e}{c^2 r_0} \frac{d^2 y(t')}{dt^2},$$

where $t' = t - r(t')/c \approx t - r_0/c + (\rho/c) \sin \omega_0 t'$ is the retarded time. Then noting that

$$\frac{dt}{dt'} = 1 - \beta \cos \omega_0 t',$$

where $\beta = \rho\omega_0/c$ is the particle's velocity, we find

$$\frac{d^2y(t')}{dt^2} = \rho\omega_0^2 \frac{\beta - \cos\omega_0 t'}{(1-\beta\cos\omega_0 t')^3}.$$

The radiation is big only for $\omega t' \approx 2n\pi$. We will take the Fourier analysis of only the pulse near $t' = 0$. For this we eliminate t' in favor of $T = t - r_0/c$. For $\beta \approx 1$ we find $t' \approx 2\gamma^2 T$, and

$$\cos\omega_0 t' - \beta \approx \frac{1 - 4\gamma^6\omega_0^2 T^2}{2\gamma^2}, \qquad 1 - \beta\cos\omega_0 t' \approx \frac{1 + 4\gamma^6\omega_0^2 T^2}{2\gamma^2},$$

and hence

$$E_y(T) \approx \frac{1 - 4\gamma^6\omega_0^2 T^2}{1 + 12\gamma^6\omega_0^2 T^2}.$$

The Fourier transform of this varies as [41]

$$E_y(\omega) = e^{-\omega/2\sqrt{3}\gamma^3\omega_0}.$$

The power spectrum of the pulse, U_ω goes as

$$U_\omega \propto E_y^2(\omega) \propto e^{-\omega/\sqrt{3}\gamma^3\omega_0} \equiv e^{-\omega/\omega_C},$$

where the critical frequency is

$$\omega_C = \sqrt{3}\gamma^3\omega_0.$$

A Fourier analysis of the pulse train [38], rather than of only a single pulse, reduces the $\sqrt{3}$ in the critical frequency to 3/2 and reveals the roll-off at frequencies below $\omega_C/3$.

An interesting question of principal is whether the path length in the magnet over which the synchrotron radiation is produced could be so short that the above expression does not apply. This is readily answered by noting that the angular distribution of the radiation has a characteristic spread of $1/\gamma$; hence the arc length L in the magnet must satisfy $L/\rho > 1/\gamma$ for our results to apply [42]. Equivalently, a magnet must provide a total bend of more than 10 μrad of a 50-GeV electron for the standard results to hold. This is satisfied, but not by too much, in our proposed beamline.

10 References

[1] F. Sauter, *Über das Verhalten eines Elektrones im homogenen elektrischen Feld nach der relativistisches Theorie Diracs*, Zeits. f. Phys. **69**, 742 (1931). See also §129, prob. 2 of ref. [4].

[2] J. Schwinger, *The Quantum Correction in the Radiation by Energetic Accelerated Electrons*, Proc. Nat. Acad. Sci. **40** (1954) 132.

[3] For a review see K.T. McDonald, *Proposal for Experimental Studies of Nonlinear Quantum Electrodynamics*, Princeton U. Report DOE/ER/3072-32 (Sept. 1986).

[4] See for instance §40 of V.R. Berestetskii, E.M. Lifshitz and L.P. Pitaevskii, *Quantum Electrodynamics*, 2nd ed., (Pergamon Press, 1982).

[5] See for instance T. Cowan and J. Greenberg, in *Physics of Strong Fields*, ed. W. Greiner (Plenum, N.Y. 1987); the original papers are J. Schweppe *et al.*, *Observation of a Peak Structure in Positron Spectra from U+Cm Collisions*, Phys. Rev. Lett. **51** (1983) 2261; T. Cowan *et al.*, *Observation of Correlated Narrow-Peak Structures in Positron and Electron Spectra from Superheavy Collision Systems*, Phys. Rev. Lett. **56** (1986) 444; P. Salabura *et al.*, *Correlated e^+e^- Peaks Observed in Heavy-Ion Collisions*, Phys. Lett. **B245** (1990) 153; W. Koenig *et al.*, *On the Momentum Correlation of (e^+e^-) Pairs Observed in U+U and U+Pb Collisions*, Phys. Lett. **B218** (1989) 12.

[6] A. Belkacem *et al.*, *New Channeling Effects in the Radiative Emission of 150 GeV Electrons in a Thin Germanium Crystal*, Phys. Lett. **B177** (1986) 211; *Photon Multiplicities in the Hard Radiation of 150 GeV Electrons in an Aligned Germanium Crystal*, Phys. Lett. **B206** (1988) 561; R. Medenwalt *et al.*, *Detailed Investigations of Shower Formation in Ge- and W-Crystals Traversed by 40-287 GeV/c Electrons*, Phys. Lett. **B227** (1989) 483.

[7] R.C. Fernow *et al.*, *Proposal for an Experimental Study of Nonlinear Compton Scattering*, Princeton U. Report DOE/ER/3072-55 (Oct. 25, 1989).

[8] See for instance M. Bell and J.S. Bell, *End Effects in Quantum Beamstrahlung*, Part. Acc. **24** (1988) 1; R. Blankenbecler and S.D. Drell, *Pair Production from Photon-Photon Collisions*, Phys. Rev. Lett. **61** (1988) 2324; M. Jacob and T.T. Wu, *Quantum Calculation of Beamstrahlung*, Nucl. Phys. **B303** (1989) 373, 389; P. Chen and K. Yokoya, *Field-Gradient Effect in Quantum Beamstrahlung*, Phys. Rev. Lett. **61** (1988) 1101; V.N. Baier, V.M. Katkov and V. M. Strakhovenko, Nucl. Phys. **B328**, 387 (1989).

[9] G. Breit and J.A. Wheeler, *Collision of Two Light Quanta*, Phys. Rev. **46** (1934) 1087.

[10] R.H. Milburn, *Electron Scattering by an Intense Polarized Photon Field*, Phys. Rev. Lett. **10** (1963) 75.

[11] H.R. Reiss, *Absorption of Light by Light*, J. Math. Phys. **3** (1962) 59; *Production of Electron Pairs from a Zero-Mass State*, Phys. Rev. Lett. **26** (1971) 1072.

[12] H. Tsertos *et al.*, *High-Sensitivity Measurements of the Excitation Function for Bhabha Scattering at MeV Energies*, Phys. Rev D **40** (1989) 1397; S.M. Judge *et al.*, *Search for Long-Lived Neutral Resonances in Bhabha Scattering around 1.8 MeV/c^2*, Phys. Rev. Lett. **65** (1990) 972.

[13] A.L. Hallin *et al.*, *A Sensitive Search for Resonances in Low Energy e^+e^- Scattering,* Princeton U. preprint (May, 1991).

[14] S.L. Adler, *A New Embedding of Quantum Electrodynamics in a Non-Abelian Gauge Structure*, Phys. Lett. **B221** (1989) 39; D.G. Caldi, , Comments Nuc. Part. Phys. **19** (1899) 137.

[15] J.E. Spencer, *High Brightness Sources for Colliders,* SLAC-PUB-5561 (May 1991).

[16] I.F. Ginzburg *et al.*, *Colliding γe and $\gamma\gamma$ Beams Based on the Single-Pass e^+e^- Collider*, Nucl. Inst. and Meth. **205** (1983) 47.

[17] J.E. Spencer and S.J. Brodsky, *Breeding New Light into Old Machines (and New)*, SLAC-PUB-3646 (1985).

[18] See for instance A.C. Melissinos, *Final Technical Report Grant AFOSR-87-0328*, University of Rochester (1991); C. Bamber, W. Donaldson, T. Juhasz, L. Kingsley and A.C. Melissinos, *Radial Compression of Picosecond Electrical Pulses*, Part. Acc. **23** (1988) 255.

[19] D. Normand *et al.*, *Focused Laser Intensity Measurement at 10^{18} Watts/cm^2 and 1053 nm*, Opt. Lett. **15** (1990) 1400.

[20] C.J.S. Damerell *et al.*, *A Vertex Detector for SLD*, Nucl.'Instr. and Meth. **A275** (1989) 484; *A CCD-Based Vertex Detector for SLD*, Nucl. Instr. and Meth. **A288** (1990) 236.

[21] G. Barbiellini *et al.*, *Energy Resolution and Longitudinal Shower Development in a Si/W Electromagnetic Calorimeter*, Nucl. Instr. and Meth. **A235** (1985) 55; G.P. Ferri *et al.*, *Silicon Detectors Used for Beam Diagnostics in the LEP Collider*, Nuc. Phys. B (Proc. Suppl.) **23A** (1991) 419.

[22] S.C. Berridge *et al.*, *Beam Test of the SLD Silicon-Tungsten Luminosity Monitor*, IEEE Trans. Nuc. Sci. **37** (1990) 1191.

[23] N.B. Narozhnyi, A.I. Nikishov and V.I. Ritus, *Quantum Processes in the Field of a Circularly Polarized Electromagnetic Wave*, Sov. Phys. JETP **20** (1963) 622; see also §101 of Ref. [4].

[24] P. Chen and V.I. Telnov, *Coherent Pair Creation in Linear Colliders*, Phys. Rev. Lett. **63** (1989) 1796; see also V.N. Baier, V.M. Katkov and V.M. Strakhovenko, Sov. J. Nuc. Phys. **14** (1972) 572.

[25] G. Bassompierre *et al.*, *Darmstadton Hunting in γ-Crystal Interaction*, Proceedings of the Jan. 1991 Moriond Conference.

[26] M. Spighel, private communication (Sept. 27, 1991).

[27] P. Maine, *et al.*, *Generation of Ultrahigh Peak Power Pulses by Chirped Pulse Amplification*, IEEE J. Quantum Electron. **QE-24** (1988) 398.

[28] Y.-H. Chuang, D.D. Meyerhofer, S. Augst, H. Chen, J. Peatross, and S. Uchida, *Pedestal Suppression in a Chirped Pulse Amplification Laser*, J. Opt. Soc. Am. **B8** (1991) 1226.

[29] D. Strickland and G.'Mourou, Opt. Comm. **56** (1985) 219.

[30] G.P. Agrawal, *Nonlinear Fiber Optics* (Academic Press, Boston, 1989).

[31] E.B. Treacy, IEEE J. Quantum Electron., **QE-5** (1969) 454.

[32] M. Pessot, P. Maine, and G. Mourou, Opt. Comm. **62** (1987) 419.

[33] A.E. Siegman, *Lasers* (University Science, Mill Valley, CA, 1986), pp. 331–361, 1171–1212.

[34] M.D. Perry, F.G. Patterson, and J. Weston, Opt. Lett. **7** (1990) 381.

[35] R.S. Craxton, *Theory of High-Efficiency Third Harmonic Generation of High-Power Nd:Glass Laser Radiation*, Opt. Comm. **34** (1980) 474; W. Seka *et al.*, *Demonstration of High-Efficiency Third Harmonic Conversion of High-Power Nd:Glass Laser Radiation*, Opt. Comm. **34** (1980) 469.

[36] Y. Wang, B. Lether-Davies, Y.-H. Chuang, R. S. Craxton, D. D. Meyerhofer, Opt. Lett., to be published.

[37] Y. Wang and R. Dragila, *Efficient Conversion of Picosecond Laser Pulses into Second-Harmonic Frequency Using Group-Velocity Dispersion*, Phys. Rev. A **41** (1990) 5645.

[38] J. Schwinger, *On the Classical Radiation of Accelerated Electrons*, Phys. Rev. **75** (1949) 1912.

[39] W.H. McMaster *et al.*, *Compilation of X-Ray Cross Sections*, UCRL-50174, Sec. II, Rev. 1 (1969).

[40] R.P. Feynman, R.B. Leighton, and M. Sands, *The Feynman Lectures on Physics*, (Addison-Wesley, Reading, MA, 1963) Chap. 34, Vol.'I.

[41] Integral 3.767.2 of I.S.'Gradshteyn and I.M. Ryzhik, *Table of Integrals, Series, and Products*, (Academic Press, New York, 1980).

[42] R. Coïsson, *On Synchrotron Radiation in Short Magnets*, Opt. Comm. **22** (1977) 135; see also V.G. Bagrov *et al.*, *Radiation of Relativistic Electrons Moving in an Arc of a Circle*, Phys. Rev. D **28** (1983) 2464.